Panakkal, P., Wyderka, A. M., Padgett, J. E., & Bedient, P. B. (2023). Safer this way: Identifying flooded roads for facilitating mobility during floods. Journal of Hydrology, 625, 130100.

https://doi.org/10.1016/j.jhydrol.2023.130100

Safer This Way: Identifying Flooded Roads for Facilitating Mobility During Floods

Pranavesh Panakkal[a], Allison M. Wyderka[a], Jamie E. Padgett[a,b], Philip B. Bedient[a]

[a] *Department of Civil and Environmental Engineering, Rice University, 6100 Main Street, Houston, 77005, Texas, USA*
[b] *Corresponding author, Email address: jamie.padgett@rice.edu*

Abstract

Severe storms and associated flooding pose a significant risk to urban mobility. Consequently, 40 to 63% of flood-related deaths are linked to roadway-related incidents in developed countries. The dynamic nature of flooding and the lack of real-time information make it challenging to sense flooding and its impact on roadways. Hence, existing state-of-the-art methods fall short of providing a robust, reliable, and affordable tool to facilitate situational awareness during storms. Such a tool is indispensable to aid emergency response, especially considering the potential increase in risk to flood exposure due to climate change and other factors. This study addresses this need by providing an open-source framework that couples real-time rainfall data, a physics-based flood model, and network and spatial analyses to sense real-time flood impact on the road transportation system. Case studies using three recent storms in Houston, Texas demonstrate the framework's ability to provide vehicle-class specific roadway conditions for even minor roads and residential streets—a problem existing approaches struggle with. Aside from road-link conditions, the framework can also estimate network-level flood impacts, such as identifying regions without access to critical facilities like hospitals, giving decision-makers a more holistic view of network performance. Further, the framework is interoperable with existing situational awareness tools and could augment their ability to sense road conditions during flooding. Finally, the proposed framework can equip flood-prone communities and emergency responders with reliable and accessible situational awareness content using open-source tools and data to promote safer mobility during flooding—a key goal of intelligent transportation systems.

Keywords: Floods, radar, urban mobility, situational awareness, emergency response, alert systems.

1. Introduction

Facilitating safe mobility by providing timely and reliable information on roadway status is one of the primary goals of an intelligent transportation system (ITS) (Guerrero-Ibez et al., 2018; Sumalee and Ho, 2018). Current ITS frameworks and research (Zhu et al., 2019; Sumalee and Ho, 2018; Guerrero-Ibez et al., 2018) predominantly focus on enhancing safety during normal operating conditions and provide insufficient information during adverse weather events such as floods (Dey et al., 2015). This limited focus is concerning because mobility-related incidents are the leading cause (40 to 63%) of flood casualties in many developed countries (Han and Sharif, 2021). Many factors such as risk-taking behavior (Jonkman, 2007; Maples and Tiefenbacher, 2009) and insufficient information on road conditions (Maples and Tiefenbacher, 2009) contribute to the high flood fatalities on roads. Further, climate change and land-use change are expected to increase the frequency and intensity of extreme flood events (Winsemius et al., 2016; Field et al., 2012). Increased flood hazard, combined with increased flood exposure (Jongman et al., 2012), could exacerbate flood-related road fatalities. These factors emphasize the need for reliable and accessible situational awareness systems for ensuring safe mobility during future flood events. Situational awareness is defined here as the real-time knowledge of the road network condition at the link and network levels.

Several studies have proposed frameworks to address the need for reliable situational awareness tools. These frameworks can be broadly categorized into two: frameworks that directly observe flooded roads using physical, social, or remote sensors, and frameworks that indirectly infer road conditions by coupling rainfall observations with mathematical flood routing models. While existing frameworks have their advantages and perform sufficiently for their use cases, they fall short of providing a comprehensive, equitable, stand-alone situational awareness tool to sense road and network level flood impacts. To elaborate, while a network of physical sensors such as automobile radar (Viikari et al., 2009), cameras (Lo et al., 2015), and water depth gages (Harris County Flood Control District, 2022a) can sense the road surface condition as well as flood inundation for an urban region, it is prohibitively expensive to deploy them at optimal spatial density due to the cost associated with deployment, operation, maintenance, and security (Jiang et al., 2018). Such expensive systems are especially unattainable for socioeconomically disadvantaged communities who are also often disproportionately affected by flooding and potential climate change impacts (Levy and Patz, 2015).

In urbanized regions with active users, social sensors such as crowdsourcing (e.g., Waze (Google LLC, 2022a)) (Praharaj et al., 2021) and social media analytics (e.g., Twitter (Twitter, Inc., 2022)) (Fan et al., 2020b) can provide superior spatial coverage than physical sensors. At the same time, they might introduce bias (Fan et al., 2020a), noise (He et al., 2017), and significant time lags between the occurrence of an event and its detection (De Longueville et al., 2009). These limitations, together with potential for misinformation and lack of quantitative flood depth estimates, render social sensors lacking as the sole source for situational awareness, especially considering that a majority of flood fatalities are caused by flash floods (Han and Sharif, 2021). Similarly, remote sensors such as satellite images (Ahmad et al., 2019) and unmanned aerial vehicles (Perks et al., 2016) might not be suitable for real-time applications due to limited availability during inclement weather, significant time lag between revisit times of satellites, and obstacles such as clouds and vegetation (Jiang et al., 2018). Synthetic Aperture Radar can potentially improve flood monitoring by overcoming some drawbacks of conventional satellite remote sensing (Carreño Conde and De Mata Muñoz, 2019; Landuyt et al., 2018). However, the time lag between revisit times still limits their application in real-time emergency response applications. Further, recent advances in deep learning and image processing (Geetha et al., 2017; Jiang et al., 2018; Chaudhary et al., 2019) offer promising methods for estimating flood depth from low-resolution images. Additional model development and testing under operational conditions such as low light, fog, and glare are required to further enhance the generalizability of image processing models. Finally, though authoritative sources such as traffic information and warning systems (Texas Department of Transportation, 2022) provide road closure alerts, the data availability is usually limited to major highways.

While direct flood observations are reliable, they are not always available; an alternative is to leverage real-time rainfall observations and physics-based flood models to infer road conditions. Though past studies have demonstrated the capability of physics-based models to estimate flood impacts (Gori et al., 2020; Coles et al., 2017; Yin et al., 2017; Green et al., 2017; Pyatkova et al., 2019; Hackl et al., 2018; Evans et al., 2020; Pregnolato et al., 2017), they primarily focused on offline applications such as vulnerability and risk assessment. Some recent studies (Panakkal et al., 2019; Mioc et al., 2015; Ming et al., 2020; Naulin et al., 2013; Versini et al., 2010; Morsy et al., 2018; Johnson et al., 2018) show that combining real-time rainfall data with flood models is a viable alternative to frameworks relying solely on direct flood observations; notably, they excel in two critical areas: availability and affordability. These studies have shown that state-of-the-art flood models can reliably estimate the flood conditions over a large area and can be built using open-source data and technologies easily accessible to most flood-prone communities (Morsy et al., 2018; Ming et al., 2020; Mudashiru et al., 2021; Brunner, 2021; National Oceanic and Atmospheric Administration, 2016).

Current frameworks that leverage flood models fail to provide a comprehensive tool for mobility-centric situational awareness. Many existing physics-based frameworks limit flood prediction to specific watchpoints in the watershed (such as bridges and roads adjacent to streams) or capture only riverine floods. For example, the National Water Model (National Oceanic and Atmospheric Administration, 2016; Johnson et al., 2019) used in Johnson et al. (2018) provides high-quality flow predictions for streams across the U.S. but does not provide pluvial flooding predictions or water velocity data, which are both critical for inferring network-level impacts of flooding and vehicle safety. Both pluvial and fluvial floods represent a considerable risk to roadway mobility in urban areas. Consequently, models capturing flood impacts on transportation throughout the watershed are essential. Further, existing frameworks also lack a scalable method to consider roadway topography (elevated vs. at-grade roads) when determining flooded roadways and thus could overestimate flood impacts.

Additionally, state-of-the-art physics-based and observation-based frameworks showed limited to no consideration of vehicle characteristics and network-level impacts of flooding (Johnson et al., 2018; Ahmad et al., 2019; Ming et al., 2020; Naulin et al., 2013; Morsy et al., 2018; Texas Department of Transportation, 2022; Google LLC, 2022a). Observing water does not imply the road is impassable to all vehicles (e.g., passenger cars vs. high-water vehicles); a road is impassable for a vehicle if flood conditions (inundation depth and flow velocity) pose a safety risk. By neglecting the vehicle characteristics in identifying flooded roads, existing methods could misclassify roads and endanger emergency responders. Similarly, while identifying flooded road links is necessary, it alone is insufficient for emergency response decision-making. Providing a holistic view of flood impacts on access to communities and critical facilities, such as hospitals, is vital for timely response and evacuation during flooding.

In conclusion, there is a need to address gaps in the current suite of situational awareness tools to enhance roadway safety under present and future flooding. Such a system, in addition to being reliable, affordable, and available with a limited time lag, should also a) be available for a majority of roads; b) be capable of identifying link- and network-level impacts of flooding; and c) consider vehicle characteristics and roadway topography to provide vehicle-specific road condition. This study addresses these needs via a new real-time situational awareness system called open-source situational awareness framework for mobility (OpenSafe Mobility).

OpenSafe Mobility leverages a physics-based flood model instead of sensors to infer flood conditions. It combines gage-adjusted radar rainfall, a rainfall-runoff flood model, and network and spatial analyses to infer flood conditions of roads and quantify the network-level flood impacts on mobility. Furthermore, while OpenSafe Mobility can function independently, it is designed to be interoperable with existing ITS frameworks via the Representational State Transfer (REST) Application Programming Interface (API) access.

2. The Proposed Architecture

This section describes the OpenSafe Mobility architecture (Fig. 1). First, real-time radar rainfall data are collected and processed to identify flood-inducing rainfall (Fig. 1a). For events that could cause flooding, a select duration of the radar rainfall data (referred to as the maximum considered duration or d_{max}) preceding the last available radar data is collected and processed (Fig. 1b). The considered rainfall duration d_{max} should be sufficient to accurately model flood impacts in the study region. Next, a physics-based rainfall-runoff flood model (Fig. 1b) uses the processed radar rainfall data to infer the current flood conditions. Flood hazards at road links and vehicle characteristics are then used to identify flooded roads for select vehicle classes (Fig. 1c). Next, OpenSafe Mobility uses the road condition data to estimate network-level impacts of road closures on roadway access to critical facilities such as fire stations and hospitals (Fig. 1d). The OpenSafe Mobility results can help find safe routes between origin-destination pairs and identify regions without access to critical facilities such as hospitals. Finally, the results are communicated to stakeholders through a web interface and REST API (Fig. 1e).

2.1. Radar Rainfall Data

For accurate flood modeling, reliable and robust real-time rainfall data that captures the temporal and spatial variability of rainfall is essential. Three common sources of rainfall data are rain gages, radar rainfall, and gage-adjusted radar rainfall (GARR). GARR fuses observations from rain gages (which on their own suffer from spatial availability) and radar data (which on its own suffers from accuracy) to provide a more complete spatial and temporal distribution of rainfall with higher reliability (Fang et al., 2011; Vieux & Associates, Inc., 2022). Consequently, OpenSafe Mobility uses GARR for real-time rainfall data. Depending on the cost and availability of the sources in the study region, OpenSafe Mobility can also be tailored to use any of the three sources.

During operation, OpenSafe Mobility acquires spatial rainfall data at regular intervals. Since all events do not produce flooding, tracking rainfall and initiating further analysis only for flood-inducing events (as indicated by exceeding a threshold) can promote optimal use of computing resources.

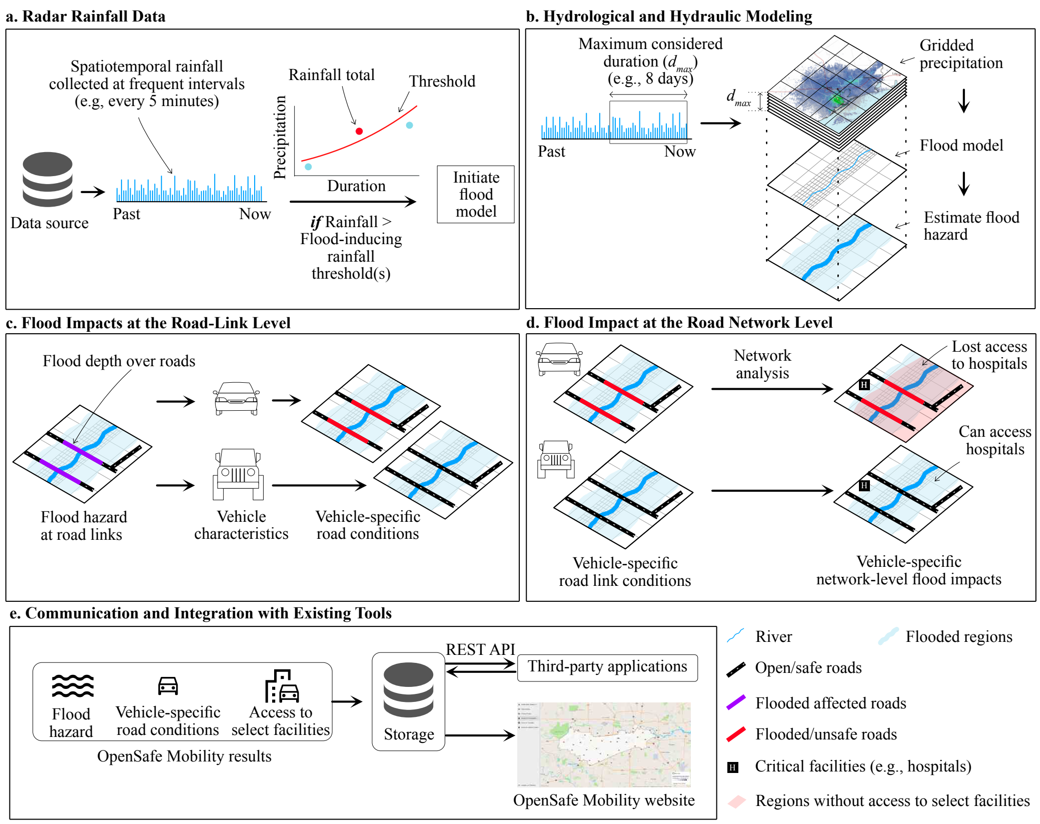

Figure 1: Overview of OpenSafe Mobility. Image source: National Weather Service (2022); Google LLC (2022b)

The threshold flood-inducing rainfall depends on the characteristics of the study region and can be obtained from either historical data or hydrological studies. In the absence of detailed hydrological studies, such as Dao et al. (2020), point precipitation frequency estimates and historical flooding in the study region can be used to define flood inducing thresholds. For example, in many parts of Houston, the stormwater network is designed to carry a 2-year storm (Haddock and Kanwar, 2021) and any rainfall exceeding the threshold (say 5-year event) could overwhelm the drainage system and result in flooding. Fig. 2 illustrates an example scenario. Here, rainfall in a Brays Bayou subwatershed region is plotted in five-minute intervals (Fig. 2a) and compared against the 5-year recurrence interval for the region from NOAA Atlas-14 (Perica et al., 2018) for each time step (Fig. 2b). The observed rainfall for the subwatershed exceeded the NOAA Atlas-14 5-year thresholds on Day 26 at 19:45 for the first time during the event. Similarly, OpenSafe Mobility monitors the entire study region and initiates the model run if the threshold is exceeded at any point within the study area or at the watershed level. Once activated, OpenSafe Mobility will continue to run the model until all roads are passable.

Once the flood-inducing rainfall threshold is exceeded, a select duration of the rainfall (referred to as maximum considered duration d_{max}) before the last available time step is used to run the flood model. The duration of rainfall considered (d_{max}) should be sufficient to estimate the flood conditions reliably. Specifically, d_{max} should be more than the time of concentration of the study region and should be sufficient to accurately capture soil moisture conditions in the watersheds and base flow in channels. Practically, d_{max} can

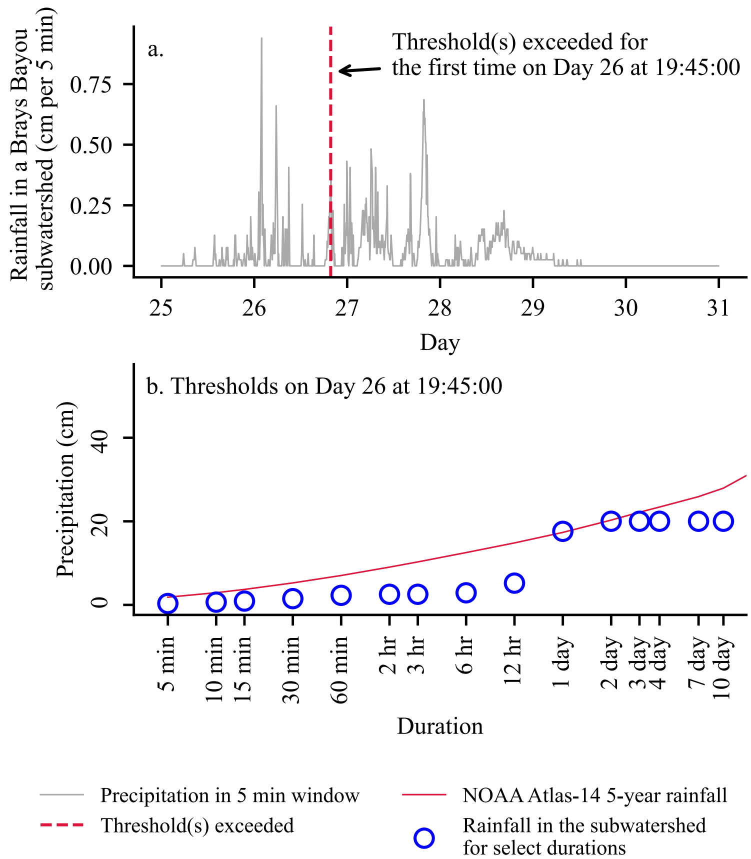

Figure 2: Example criteria for identifying flood-inducing rainfall. Here NOAA Atlas-14 5-year (20% annual probability of exceedance) recurrence interval rainfall thresholds (red line in part b) are used to initiate OpenSafe Mobility model run. The red dotted line (part a) marks the first-time step for which rainfall amounts exceeded any thresholds (red line in part b) in a select subwatershed. The rainfall totals corresponding to this time are compared against different thresholds in the bottom image (part b). OpenSafe Mobility monitors rainfall in every part of the watershed and initiates the model runif the threshold is exceeded in any location within the study area. Data sources: NOAA Atlas-14 Perica et al. (2018) and Vieux & Associates, Inc.

be identified by varying duration of rainfall considered for select historical storms and checking model accuracy using historical data at select watch-points in the study area. Maximum event duration d_{max} selected should also consider acceptable time lag for real-time situational awareness application. The acceptable time lag depends on stakeholder needs. For emergency response applications, a limited time lag (e.g., $\leq$ 30 min) is preferred to ensure the pertinency of the model predictions. The time lag consists of the time required to acquire rainfall data, process the radar, run the OpenSafe Mobility model, and publish the results. Out of these steps, the time to acquire the rainfall data and run the OpenSafe Mobility model is typically time-consuming. The time required to acquire rainfall data depends on the data source and is beyond the control of OpenSafe Mobility. The model runtime depends on the duration of rainfall, resolution of the model, study area size, and the computing resources available. Once d_{max} and acceptable time lag are identified, factors such as computing resources available and the resolution of the flood and network models are optimized to maximize model accuracy and reduce lag time. Considering an event duration less than d_{max} might be necessary for larger study areas to provide approximately correct results within an acceptable time lag. For applications with longer model run time, deploying multiple machines that can asynchronously process the radar data can significantly improve data availability. Further, it would be ideal if these machines were not co-located as flood events could result in large-scale network and power outages.

2.2. Hydrological and Hydraulic Modeling

During flood analysis, hydrological and hydraulic analyses are performed using the input rainfall data and a calibrated 2D unsteady flow model. While several capable tools exist for 2D unsteady flow modeling (Mudashiru et al., 2021), this study uses Hydrologic Engineering Center-River Analysis System (HEC-RAS) software (version 6.0) (Brunner, 2021) from the United States Army Corps of Engineers (USACE) for flood modeling. The widespread adoption of HEC-RAS among industry (Dysarz, 2018), government agencies (Harris County Flood Control District, 2022b), and academia (Gori et al., 2020; Mudashiru et al., 2021) is especially appealing as it could facilitate easy adoption and transferability of OpenSafe Mobility. OpenSafe Mobility will leverage HEC-RAS to model both local street level (pluvial) flooding and riverine (fluvial) flooding using gridded rainfall data. Please refer to the HEC-RAS flood manual (Brunner, 2021) for more details on HEC-RAS.

While the version of OpenSafe Mobility presented here uses HEC-RAS, any tool that meets the following criteria can be used for real-time rainfall-runoff analysis: a) the model should efficiently perform 2D unsteady flow analysis using real-time rainfall data, accurately capturing pluvial and fluvial flooding; b) the model should generate water surface elevation and flow velocity data at a suitable resolution to discern road conditions; and c) the model should provide automated workflows (via code or APIs) to initiate model run and extract results. Several such tools are available in the literature, and Mudashiru et al. (2021) present a brief overview of flood mapping methods and tools.

To ensure model accuracy, the model is calibrated using select historical rainfall events in the study regions and tested on unseen storms to ensure generalizability. During calibration, model parameters are iteratively modified until model outputs converge to the observed stream gage readings.

2.3. Using Flood Hazard Data to Estimate Vehicle-Specific Road-Link Conditions

The flood model uses the gridded rainfall data to perform hydrological (rainfall-runoff simulation) and hydraulic (flow routing) simulations to infer the current flood conditions. Example variables that can quantify the flood conditions include water depth over the terrain, water surface elevation, and flow velocity. While many studies use water depth estimates to identify flooded roads, this method could introduce errors, particularly for elevated roads and bridges. The water depth map from a flood model represents the water over the bare earth surface without infrastructure elements like elevated roads and bridges. This study subtracts the elevation of roads, derived from Light Detection and Ranging (LiDAR) point clouds data, from water surface elevation data from the flood model to estimate flood depths over roads (d^r). Fig. 3 shows an example of LiDAR point cloud data obtained from an aerial survey (Houston-Galveston Area Council, 2022) and Fig. 4 illustrates the difference between DEM used for flood analysis and a digital surface model (DSM) developed from LiDAR data that preserves roadway elevation.

OpenSafe Mobility provides three strategies to estimate road link status: depth-centric, probabilistic depth-centric, and stability-centric approaches. These strategies are intended to address the variability in stakeholder needs, data availability, and computing resources.

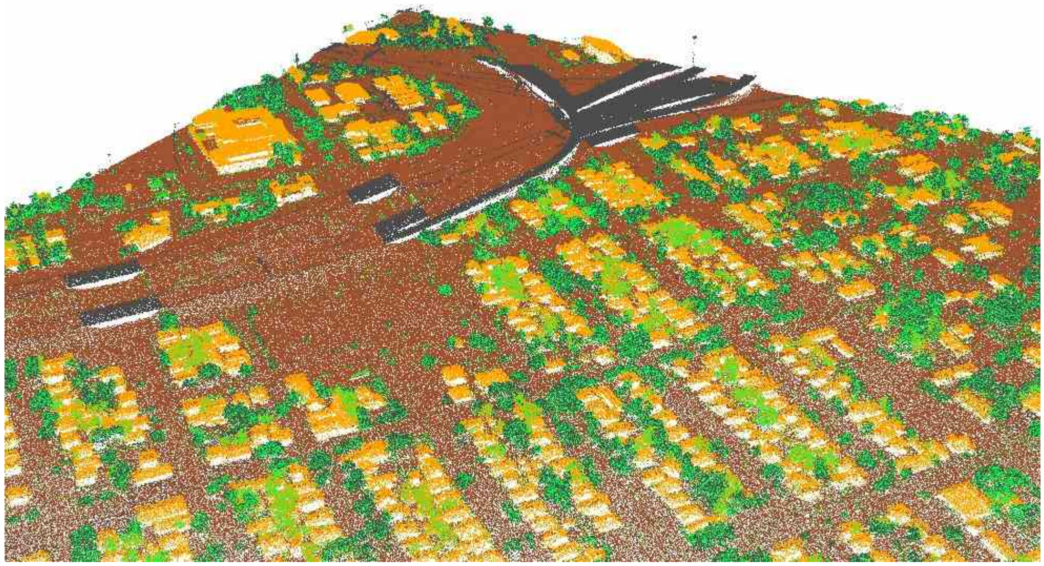

Figure 3: An example LiDAR point cloud data. Here, each point represents the elevation of that point relative to a datum. The points are color coded to categorize the point; green points indicate vegetation, yellow indicates buildings, brown indicates bare earth, and black indicates road infrastructure. Image created using LAStools (Rapidlasso GmbH, 2012). Data source: Houston-Galveston Area Council (2022).

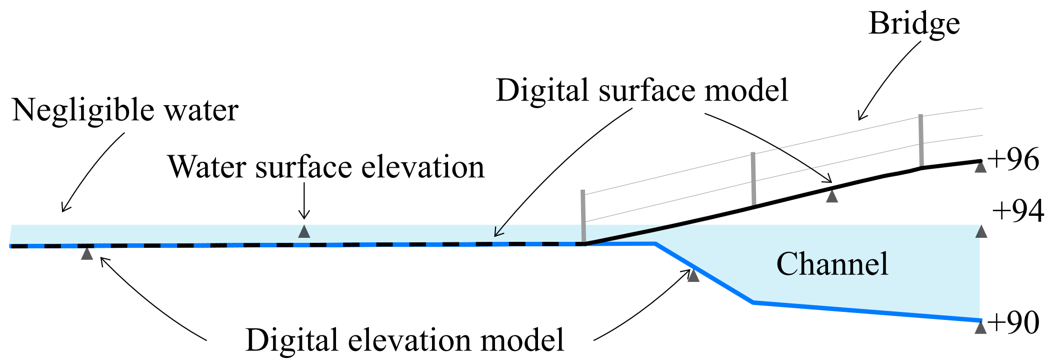

Figure 4: Comparison between a hydrologically conditioned digital elevation model (DEM) and digital surface model (DSM). Infrastructure facilities such as bridges are removed during the creation of DEM. Hence, using DEM for estimating road condition could lead to error. Alternatively, subtracting DSM from water surface elevation can reliably infer roadway condition.

2.3.1. Depth-Centric Approach to Estimate Road Link Status

In the depth-centric approach (Fig. 5a-d; Eq.1), safe wading height (w_h) of vehicles (Contreras-Jara et al., 2018) are compared against the water depth over roads (d^r) to estimate vehicle-specific roadway status (R^d). A road is not traversable if the safe vehicle wading height is less than the sum of water depth over the road and a water depth buffer (δ_d). The water depth buffer is optional, and it provides a margin to compensate for any depth underestimation from the flood model or an additional margin to assure vehicle safety.

$$R^d(d^r, \delta_d, w_h) = \begin{cases} open, & \text{if } w_h \geq d^r + \delta_d \\ closed, & \text{otherwise} \end{cases} \tag{1}$$

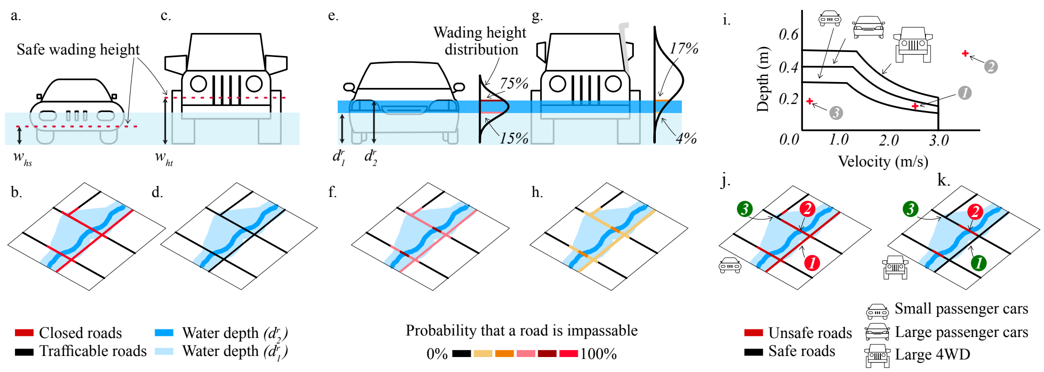

Figure 5: Depth-centric (parts a-d), probabilistic depth-centric (parts e-h), and stability-centric (parts i-k) strategies for identifying impassable roads. In the depth-centric strategy, impassable roads are identified by comparing the wading height of the vehicle with the water depth. In the probabilistic depth-centric approach, the wading height distribution of a vehicle class is used to estimate the probability of road link flooding. In the stability-centric approach, stability criteria are used to identify unsafe roads.

2.3.2. *Probabilistic Depth-Centric Approach to Estimate Road Link Status*

In the probabilistic depth-centric approach (Fig. 5e-h; Eq. 2), depth over roads (d^r) and wading height distribution (W_h)(Contreras-Jara et al., 2018) of different vehicle classes (e.g., SUVs, passenger cars) are used to estimate the probability of a road link being impassable. Here, the probability of a road link being impassable for a vehicle class (P^d) is defined as the percentage of vehicles with wading heights lesser than the water depth over the road link plus an optional buffer (δ_d) (i.e, $d^r + \delta_d$).

$$P^d(d^r, \delta_d, W_h) = \int_{-\infty}^{d^r+\delta_d} W_h(x)\, dx \tag{2}$$

2.3.3. Stability-Centric Approach to Estimate Road Link Status

The buoyancy and drag forces exerted by flood waters may cause vehicles to float, slide, or overturn. Ignoring flow velocity and focusing solely on flood depth may underestimate flood risk to vehicles. Past studies (Martnez-Gomariz et al., 2018; Shand et al., 2011; Bocanegra et al., 2020) have developed stability criteria to identify dangerous roads by considering vehicle characteristics and flood conditions (primarily flood depth and flow velocity). In the stability-centric approach, OpenSafe Mobility uses flood depth over roads (d^r) and flow velocity (v) estimates from the flood model to identify unsafe roads for a vehicle class. Any stability criteria that quantify vehicle stability using flood depth and flow velocity can be adopted in OpenSafe Mobility. Fig. 5i-k (and Equation 3) show example stability criteria (S^{dv}) from the Australian Rainfall and Runoff (AR&R)(Shand et al., 2011) for three classes of vehicles—small passenger cars, large passenger cars, and large 4WD vehicles.

$$S^{dv}(d^r, v) = \begin{cases} safe, & \text{if } d^r.v \leq s^v \ and \\ & \quad d^r \leq d^{max} \ and \\ & \quad v \leq v^{max} \\ unsafe, & \text{otherwise} \end{cases} \tag{3}$$

where:

d^{max}=0.3m; v^{max}=3m/s; s^v=0.3m^2/s for small passenger cars;

d^{max}=0.4m; v^{max}=3m/s; s^v=0.45m^2/s for large passenger cars; and

d^{max}=0.5m; v^{max}=3m/s; $s^v = 0.6$m^2/s for large 4WD vehicles.

Fig. 5 shows an example road condition map using the three proposed strategies. Depth-based strategy is used to identify roads impassable (Fig. 5b,d) for two vehicles with different wading heights (Fig. 5a,b). The probabilistic depth-based strategy is used to determine the probability of a road link being impassable (Fig. 5f,h) for two vehicle classes (Fig. 5e,g). Finally, AR&R stability criteria (Fig. 5i) is used to identify unsafe roads for small passenger cars (Fig. 5j) and large 4WD vehicles (Fig. 5k). The vehicle classes and their characteristics (safe wading height, wading height distribution, and stability criteria) are input to the OpenSafe Mobility framework; Fig. 5 illustrates some example vehicle classes and data that community members could use within the OpenSafe Mobility framework. Given information on vehicle characteristics, OpenSafe Mobility can estimate vehicle-specific road-link conditions.

Probabilistic depth-based criteria are suited for identifying potentially impassable roads and proactively initiating road closures by organizations responsible for managing flood response. Stability-based and depth-based strategies are ideal for identifying impassable roads considering individual vehicle characteristics and flow conditions. Here, vehicle-specific road condition maps can be developed using vehicle-specific depth or stability (Martnez-Gomariz et al., 2017) criteria. Such maps are especially suited for emergency response vehicle selection and routing. While stability-based criteria are more comprehensive, it introduces additional computational cost for estimating flow velocity and consequently increases model runtime and time lag. The stability-based strategy should be preferred over the depth-based strategy, especially for regions that are predisposed to experience higher flow velocity over roads during floods.

2.4. Vehicle-Specific Network-Level Impacts of Flooding on Access to Select Facilities

While identifying road conditions will facilitate safer mobility, link-level data alone is insufficient for emergency response situational awareness; identifying isolated regions with limited access to critical facilities such as hospitals, dialysis centers, fire stations, and evacuation routes are essential for prioritizing emergency response. The network-level impacts can be quantified using real-time network analysis incorporating road conditions. The OpenSafe Mobility methodology for quantifying network-level impacts of flooding is shown in Fig. 6. First, the topology of the road network is represented as a graph $G = (V, E)$, where V is a set of nodes representing points of interest such as road intersections and access locations, and E represents a set of road links connecting nodes. Next, baseline connectivity between every node in the network to the nearest facility is estimated for a select critical facility group k (e.g., all hospitals). For example, $D^n_{x\to k}$ represents the shortest distance between a node x to the nearest facility in k (e.g., the closest hospital) in the original road network. During flooding, impassable links (v^f_t) and inundated nodes (e^f_t) are removed to create an updated road network $G^f_t = (V_t, E_t)$, where $V_t = (V - v^f_t)$ and $E_t = (E - e^f_t)$ at time t. The methodology to identify impassable links depends on the strategy adopted to determine road link status (Section 2.3). For the depth-centric strategy (Eq. 1), any closed roads (i.e., $R_d = closed$) are removed; for the stability-centric strategy (Eq. 3), all unsafe roads (i.e., $S^{dv} = unsafe$) are removed. For the probabilistic depth-centric strategy (Eq. 2), a threshold probability of the link being impassable for a select vehicle class (say, 5%) is chosen, and any road links that exceed the selected threshold are removed (i.e., links with $P^d \geq 5\%$ are removed).

After removing impassable roads, the updated network is used to estimate the shortest distance ($D^t_{x \to k}$) between node x to the nearest facility in k at time t (Dijkstra, 1959). Next, connectivity loss ($CL^t_{x \to k}$) ratio (Gori et al., 2020), defined as $1 - D^n_{x \to k}/D^t_{x \to k}$ for facility k and node x at time t, is used to quantify flood impact on access to the facility group k. $CL^t_{x \to k}$ ratio varies between 0 and 1, with zero denoting no impact of flooding on the network access and one denoting complete loss of access. Finally, the node-level results can be aggregated at a geographical unit level, such as Census Tracts, to visualize the spatial distribution of flood impacts on access to a facility type. Connectivity loss maps can be generated for various critical facilities such as fire stations, dialysis centers, and shelter locations; such maps can provide a comprehensive view of flood impact on network access and assist decision-makers in identifying vulnerable regions and prioritizing emergency response actions. Finally, the OpenSafe Mobility framework can be easily extended to consider other accessibility measures (Faturechi and Miller-Hooks, 2015).

2.5. Communication and Integration with Existing Intelligent Transportation Systems

OpenSafe Mobility outputs include flood inundation maps, road conditions for different classes of vehicles, and the spatial distribution of flood impacts on access to select critical facilities such as evacuation routes, hospitals, pharmacies, and fire stations. These results are published via a website

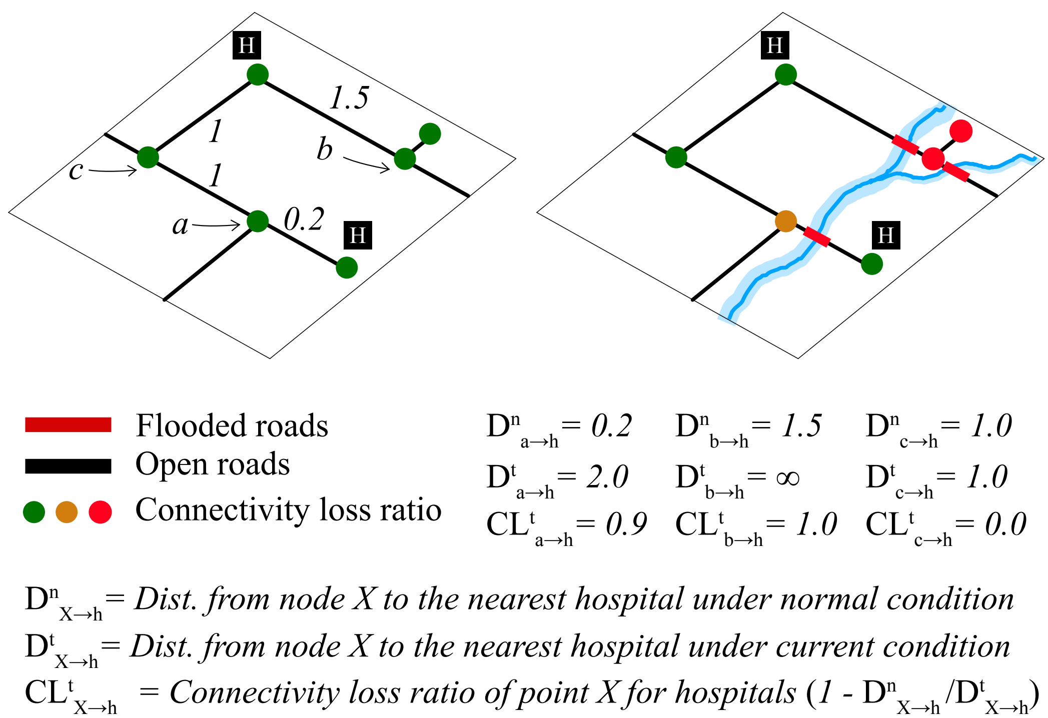

Figure 6: The methodology used to quantify network level impact of flooding on access to critical facilities. Here, connectivity loss ration is used to quantify flood impact on access between nodes in the network to the nearest critical facility.

to facilitate easy access to stakeholders (Fig. 1e). In addition to providing a stand-alone website, OpenSafe Mobility also aims to augment existing situational awareness tools and intelligent transportation systems. Towards that goal, the OpenSafe Mobility framework also provides REST API access to the generated results (Fig. 1e). Any existing or future tools could acquire real-time georeferenced results from OpenSafe Mobility thorough REST API calls. By interfacing with existing situational awareness tools OpenSafe Mobility can significantly enhance situational awareness during flooding and facilitate safer mobility.

Table 1 summarizes the input data needed for the OpenSafe Mobility framework and example data sources. Before deploying OpenSafe Mobility, it is essential to identify the data and stakeholder needs as well as to develop and test flood and network analysis models.

3. Experimental Evaluation

This section presents the experiments designed to validate OpenSafe Mobility and critically evaluate it for strengths and limitations. A case study OpenSafe Mobility framework is deployed for the Brays Bayou Watershed area in Houston, Texas. The deployed framework is then evaluated using select recent historical storm events in the watershed. For each storm event, OpenSafe Mobility model predictions are compared to ground observations to quantify model performance. The following subsections describe the experimental design in detail.

Table 1: Summary of input data required for the OpenSafe Mobility framework

Component	Data	Example data source or comment
Radar Rainfall Data and Initialization		
Acceptable time lag		Based on stakeholder need (e.g., $\leq$ 30 min)
Flood inducing rainfall threshold		Based on hydrological studies (Dao et al., 2020), or historical data, or precipitation frequency estimates (Perica et al., 2018)
Maximum considered duration (d_{max})		Based on model runtime and stakeholder needs (e.g., 8 days)
Computation resources		Stakeholder input
Rainfall data (GARR)		NEXRAD; Vieux & Associates, Inc.
Hydrological and Hydraulic Modeling		
Model building	Terrain data	Houston-Galveston Area Council (2022); U.S. Geological Survey (2023)
	Land use data	National Land Cover Database (NLCD) (Wickham et al., 2021)
	Soil data	Soil Survey Geographic Database (SSURGO) (Natural Resources Conservation Service, 2023)
	Bathymetry	Survey data (e.g., available in the hydraulic models from Harris County Flood Control District (2022b))
Model testing	Historical storms	NEXRAD; Vieux & Associates, Inc.; Iowa State University (2022); Harris County Flood Control District (2022a)
	Flood observations	Newspaper; social media; City of Houston (2022); Harris County Flood Control District (2022a); U.S. Geological Survey (2022b); TranStar (2022)
Flood Impacts at the Road-Link Level		
Road network	Road data	OpenStreetMap contributors (2017)
	Digital Surface Model	Houston-Galveston Area Council (2022)
Vehicle data	Vehicle database	Stakeholder input
	Safe wading height	Stakeholder input; owners manuals; Kramer et al. (2016)
	Wading height dist.	Stakeholder input; Contreras-Jara et al. (2018)
	Stability criteria	Martnez-Gomariz et al. (2018); Shand et al. (2011); Bocanegra et al. (2020)
Flood Impact at the Road-Network Level		
Census tract		U.S. Census Bureau (2022)
Location of select critical facilities		U.S. Department of Homeland Security (2022)
Communication and Integration with Existing Tools		
Web-hosting, cloud storage, and REST API		Amazon Web Services, Google Cloud Platform, etc.

3.1. Study Area

Houston, and specifically the Brays Bayou Watershed, is an ideal region for a case study of OpenSafe Mobility. Houston's location in the hurricane-prone Gulf of Mexico region, flat topography with little relief features (Sebastian et al., 2017), insufficient storm drainage network capacity (Haddock and Kanwar, 2021), lack of zoning laws (Sebastian et al., 2017), rapid urbanization (Zhang et al., 2018), and land-use change (Fang et al., 2014; Sebastian et al., 2017) renders it amongst the most vulnerable urban regions in the world (Chakraborty et al., 2019) for flooding. The flood risk was evident during several recent storms that wreaked havoc, especially to the transportation network. Any disturbance to the transportation network is especially detrimental to Houstonian's access to medical facilities concentrated in the Texas Medical Center (TMC) region. The TMC, the world's largest medical center, sites a majority of health care facilities and is located in the Brays Bayou Watershed in Houston. Historically, the TMC facilities were either damaged (Fang et al., 2014) or lost connectivity to flooded regions (Gori et al., 2020) during major storms. Since situational awareness information related to healthcare access is critical for emergency response, Brays Bayou Watershed, which includes the TMC region, is selected for the case study.

Brays Bayou Watershed (329 km^2 or 127 square miles) is a densely populated area southwest of Downtown Houston (Fig. 7). Brays Bayou, the main channel, begins in Fort Bend County and meets the Houston Ship Channel near Downtown Houston. The banks of Brays Bayou and its tributaries are highly developed and densely populated. Due to impervious surfaces and concrete lined channels, the watershed is prone to flash flooding, posing a significant risk to the transportation infrastructure. Consequently, the watershed was flooded during Tax Day flood (2016), Hurricane Harvey (2017), Tropical Storm (TS) Imelda (2019), and TS Beta (2020).

3.2. Flood Events and Experiment Design

Ideally, a situational awareness framework should be deployed first, and the long-term performance should be assessed through successive storms. In the absence of past performance data, this study will reenact four storms in OpenSafe Mobility and quantify model performance by comparing OpenSafe Mobility predictions to the recorded ground conditions. The selected storms are the Tax Day Flood (2016), Hurricane Harvey (2017), TS Imelda (2019), and TS Beta (2020). Hurricane Harvey's unprecedented rainfall intensity, duration, and spatial extent; Imelda's signature tri-peak pattern; and Beta and Tax Day Flood's flash flooding all pose unique challenges for situational awareness frameworks. Testing OpenSafe Mobility's efficacy during these storms facilitates a critical examination of its performance.

The Tax Day Flood (16-17 April 2016) (Nielsen and Schumacher, 2020) was a flash-flood-inducing high-intensity, short-duration event that hit southeastern Texas. Several areas of Harris County received up to 400 mm of rain. The ensuing flooding damaged more than 10,000 homes and 40,000 vehicles. The second case study storm, Hurricane Harvey (25 August to 2 September 2017) (Blake and Zelinsky, 2018) was a slow-moving hurricane that hovered near the Houston region for days, resulting in record-breaking rainfall. Unprecedented floods followed and damaged more than 300,000 structures and 500,000 cars. Importantly, the inundated roadways and the paucity of real-

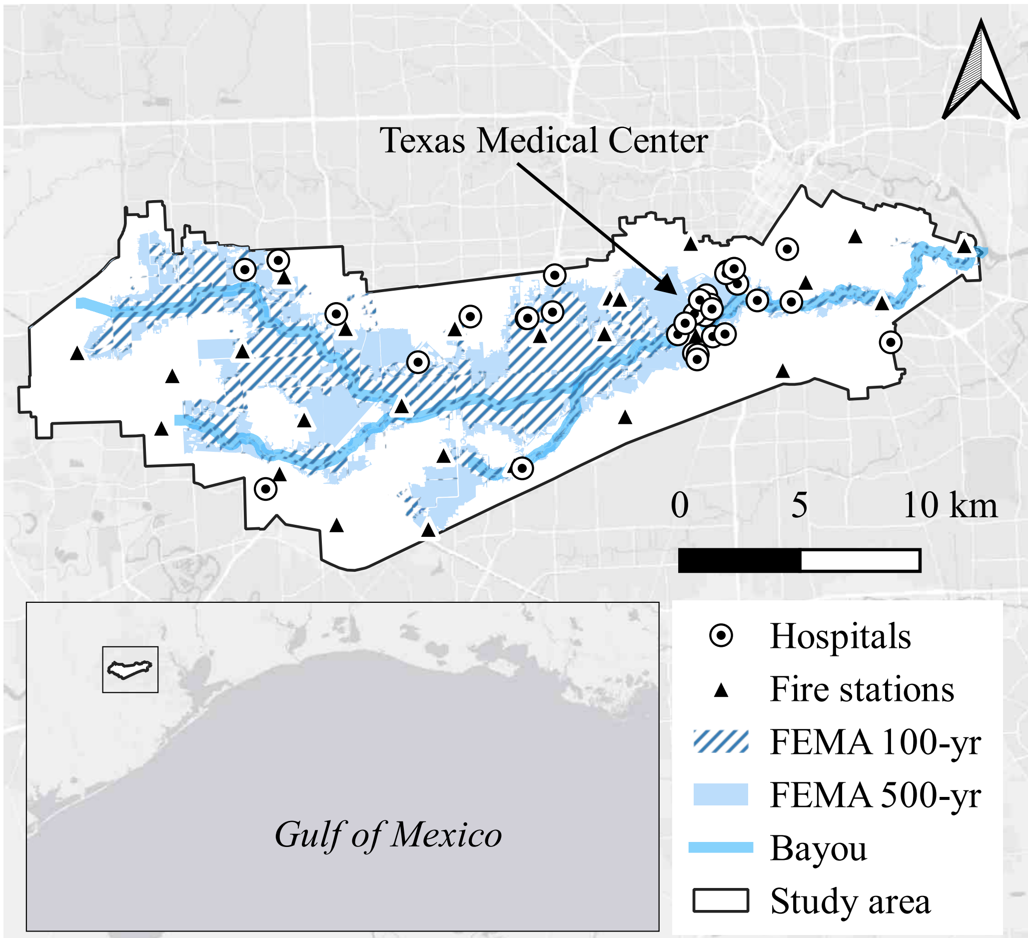

Figure 7: The study area, Brays Bayou Watershed, Houston, Texas, with the 100-year and 500-year flood plains. The 500-year flood plain represents an area with a 0.2 percent annual probability of flood exceedance. Many critical facilities such as hospitals and fire stations are located within the 500-year flood plain. Data sources: Esri (2022), FEMA (2022), U.S. Department of Homeland Security (2022), and Harris County Flood Control District (2022b).

time information on road network conditions crippled emergency response operations. The third storm, TS Imelda (17-20 September 2019) (Latto and Berg, 2020), dropped significant rain over various portions of Houston, albeit it was less intense than Harvey in the Houston area. More than 8200 homes and 4500 roads were flooded, resulting in $5 billion in losses. Finally, TS Beta (21-25 September 2020) (Beven and Berg, 2021) is the most recent among case study events. Beta was not as intense as the other case study storms, but it still caused more than $225 million in damages.

The four case study storms are used to design three sets of experiments. In the first experiment, a flood model named $M1$ is calibrated on Tax Day Flood and validated for Hurricane Harvey. In the second experiment, a new flood model $M2$ is calibrated using Tax Day Flood and Hurricane Harvey and validated using TS Imelda and Beta. In the last experiment, Model $M3$ is calibrated using all four storms in order to produce a robust model capable of handling a variety of future storms. The model $M3$ is then deployed to perform real-time analysis in the watershed since September 2021. Model calibration mainly consisted of adjusting overland and channel Mannings n values. Additionally, changes to the mesh/grid were also made during calibration, such as adjusting the cell size and alignment. The calibration of the model occurs prior to its use in the framework. The model is calibrated for each experiment only using the data available before the validation storm, assuring temporally consistent experiments. The only exception is the use of the updated 2018 LiDAR instead of 2008 LiDAR data for $M1$ and $M2$ models. Brays Bayou Watershed went through significant structural changes due to Project Brays—a watershed redevelopment program from Harris County

(Harris County Flood Control District, 2022c). Neglecting these changes could produce incorrect model results.

3.3. Physics-Based Flood Models

This study utilizes HEC-RAS version 6.0, which conducts hydrologic and hydraulic calculations in one with its 2D rain-on-grid functionality. The 2D model takes input spatiotemporal rainfall data and calculates the water surface elevation and flow velocity data necessary for determining road conditions. A 2D model was chosen for this study due to its ability to capture both fluvial (riverine) and pluvial (local) flooding. Additionally, the 2D hydraulics are unsteady (rather than steady-state), allowing the model to account for any complex hydraulics or backwater effects arising from the flat topography of the bayou. To model the hydrologic process, rainfall and infiltration data are required. Gage-adjusted radar rainfall data at the subbasin level was used for Hurricane Harvey, TS Imelda, and TS Beta and was obtained from Vieux & Associates, Inc. (2022). For the Tax Day Flood, gage-adjusted Next Generation Weather Radar (NEXRAD) (Iowa State University, 2022) was used and is provided at the 1 km^2 resolution. To model infiltration, soil data from the Natural Resources Conservation Service at a resolution of 30m x 30m was utilized and the Green & Ampt infiltration method was selected. Model parameters used were based off the HEC-RAS manual (Brunner, 2021) as well as from Harris County Flood Control District's (HCFCD) HEC-HMS model (Harris County Flood Control District, 2022b). Additionally, imperviousness data was included in the model at the subbasin level, with imperviousness values taken from HCFCD's HEC-HMS model.

The basis for hydraulic modeling in HEC-RAS 6.0 2D is a computational mesh, terrain, and land use data. The mesh consists of mainly 137 m x 137 m (450 ft x 450 ft) squares, except in channel areas, where the mesh is refined to contain roughly 30.5 m x 30.5 m (100 ft x 100 ft) cells. HEC-RAS does not treat each cell as having a single elevation but is instead able to capture the underlying terrain in each cell, creating detailed elevation volume/area relationships of each cell. The faces of each cell are essentially treated as cross-sections in that detailed elevation versus area, wetted perimeter, and roughness relationships are defined for each face of each cell (Brunner, 2021). This allows larger cell sizes to be used without compromising accuracy or resolution, thereby lowering the computational time. The boundary conditions for the 2D area are based on normal depth conditions. Land use data at a resolution of 30m x 30m was obtained from the 2016 National Land Cover Database (NLCD) (Wickham et al., 2021) and provides the basis for Manning's n values, which relate surface roughness to flow rate. While the NLCD also provides 2019 land use data, 2016 data was selected to better match the calibration events. Because Brays is already highly developed, there is negligible difference in the two datasets. 2018 HGAC LiDAR (Houston-Galveston Area Council, 2022) data was used for the terrain data set. Since LiDAR data is unable to capture channel bathymetry well, cross-section elevation data from HCFCD's current HEC-RAS model of Brays (Harris County Flood Control District, 2022b) was interpolated in the channel and used instead of LiDAR data in the channel.

OpenSafe Mobility's ability to detect road conditions throughout the watershed depends on the performance of the flood model to capture both pluvial and fluvial flooding. The model calibration and validation for fluvial flooding is shown in Appendix A and demonstrated acceptable accuracy (for example, the Nash-Sutcliffe Model Efficiency Coefficient for validating Hurricane Harvey exceeded .85 at all gages). Further, the main sections of the paper focus on validating pluvial flooding (for inferring roadway conditions away from the bayous) and road conditions.

3.4. Spatial Model Performance

Model performance for pluvial floods is quantified by comparing OpenSafe Mobility model predictions to flood observations from the City of Houston (CoH) 311 data (City of Houston, 2022). Residents can report flooding and request services like debris removal through the City of Houston's citizen service portal. The spatial location and the reported time of these flood reports are used in this experiment to validate OpenSafe Mobility.

Fig. 8a depicts the temporal distribution of 311 flood reports during Hurricane Harvey. Fig. 8b-d present the spatial distribution of the 311 flood data with the flood inundation map for that time step from $M1$. Fig. 8e shows the spatial distribution of all flood reports from 311 data (385 observations) for Hurricane Harvey. Similarly, Fig. 8f-j show 311 data (29 observations) for TS Imelda and model predictions from $M2$, while Fig. 8k-o show 311 data (32 observations) from TS Beta and model predictions from $M2$.

For each flood report in the 311 data, the most recent depth map is used to infer the condition within a buffer radius of the flood report. A buffer radius is used as many 311 locations are geocoded using standardized addresses, and in many cases, residents will report street flooding even when their parcel is not flooded. Streets are susceptible to flooding due to the

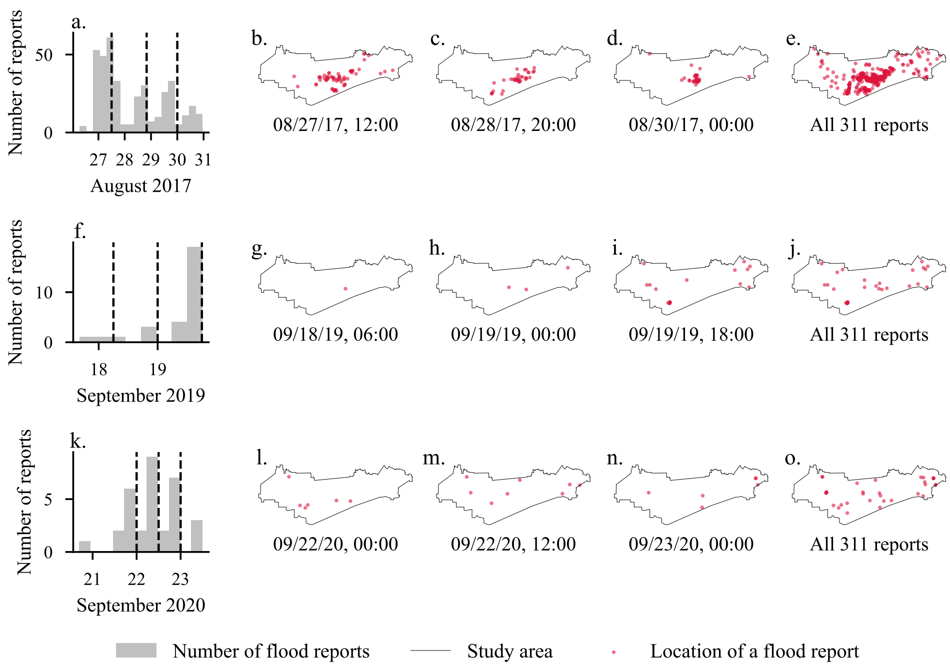

Figure 8: Location of flood reports from 311 call database. Parts a, f, and k show the temporal distribution of flood reports during Hurricane Harvey, Tropical Storm Imelda, and Tropical Storm Beta. Parts b-d show the location of flood reports for three timestamps and Part e shows all flood reports for the event duration. Data sources: City of Houston (2022) and Harris County Flood Control District (2022b).

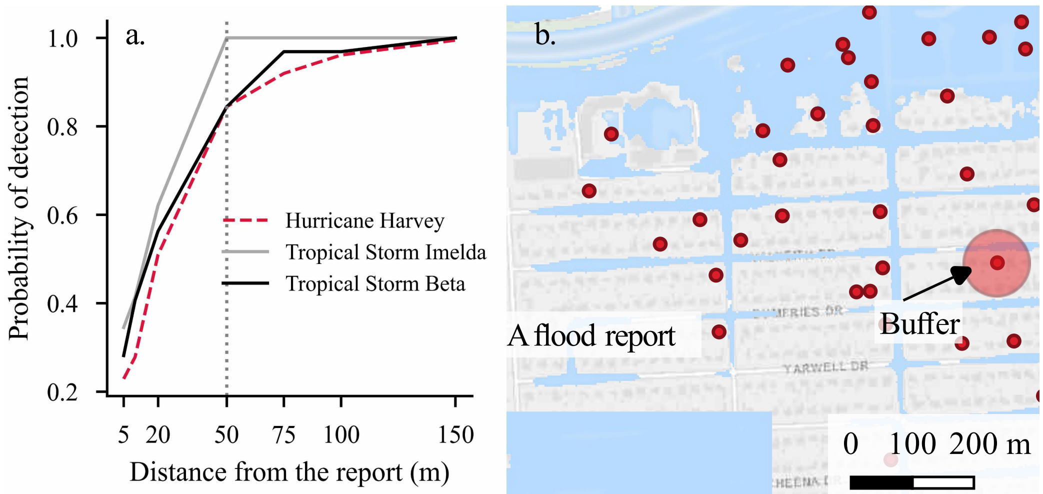

Figure 9: OpenSafe Mobility model performance for detecting flooding for three case study storms. Results indicate that OpenSafe Mobility can reliably capture spatial distribution of flooding. Data sources: Esri (2022) and City of Houston (2022).

clogging of stormwater networks and their lower elevation compared to the adjacent regions. Fig. 9b shows an example buffer around a flood report. It is evident that though the reported location is dry, the adjoining street is flooded.

Probability of detection (PoD) is used to measure model performance in this experiment and is the proportion of actual flooded cases (311 reports) that the model correctly identified. PoD ranges from 0 to 1, and a higher value indicates superior model performance. The PoD of a model depends on the buffer distance. For example, in Fig. 9a, as the buffer distance increases from 5 m to 150 m, the PoD increases from 20 percent to 100 percent. Studying model performance indicates that in all three flood events, OpenSafe Mobility could detect flooding for at least 80 percent of the cases within a buffer of 50 m. Further, for a buffer of 150 m, the models could detect flooding for nearly all 311 reports. Further visual inspection reveals that false-negative flood reports at a buffer typically represent scenarios where flooded locations are encoded using conventional addresses adjacent to a flooded street. This experiment demonstrates OpenSafe Mobility's capacity to model fluvial and pluvial flooding reliably.

3.5. Quantitative Model Performance

This section assesses OpenSafe Mobility's ability to provide reliable water depth estimates by comparing OpenSafe Mobility model predictions to traffic camera data (Fig. 10) and USGS high water level marks (HWLMs) (Fig. 11). HWLMs report the maximum water level observed at points without information on observation time. In contrast, while traffic camera data from Houston TranStar provides the observation time, it doesn't give a quantitative estimate of flood depth, necessitating qualitative flood depth inference from images.

Fig. 10 compares the flood depth estimates from traffic cameras to OpenSafe Mobility ($M1$ for Hurricane Harvey; $M2$ for TS Imelda and Beta) flood estimates at the time of observation. Flood depths from images are estimated by comparing the flooded scene to its normal dry condition. Due to the inability to determine an exact flood depth, a most likely value (represented by a dot) and the lower and upper bounds of flood depths (represented by error bars) are reported. The results for Hurricane Harvey (mean error (ME) = 0.16, mean absolute error (MAE)=0.48, root mean square error (RMSE)=0.74 (Botchkarev, 2019) for 10 observations) indicate that for Harvey, the OpenSafe Mobility model provides a reasonable estimate of flood depth. Here, mean error (ME) is defined as $1/n \sum_{j=1}^{n} e_j$ where

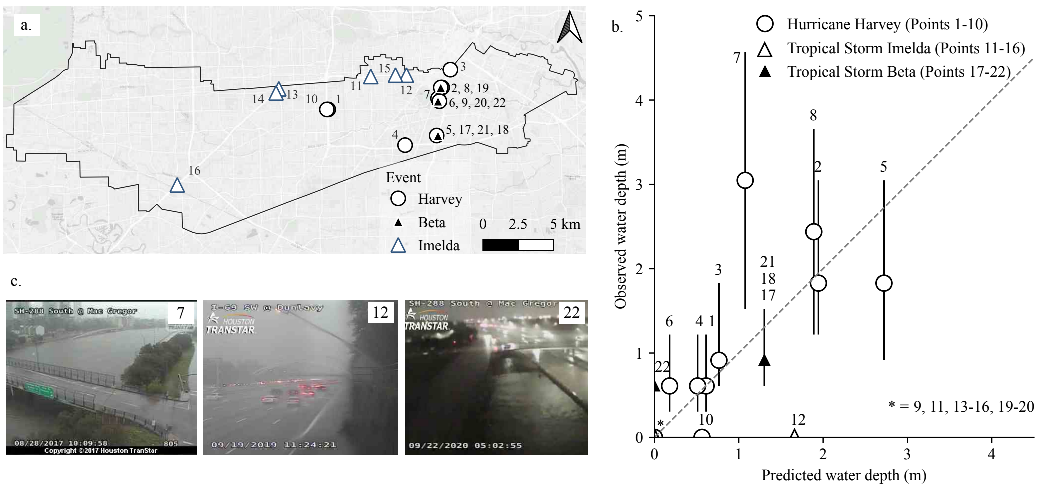

Figure 10: Comparisons of observed flood depths from traffic camera data to OpenSafe Mobility model predictions. Part a maps the locations of the traffic camera data; part b compares the flood depth estimated from images to OpenSafe Mobility predictions; and part c offers some example traffic camera images. Error bars (part b) represent potential lower and upper bounds in the depth estimate from images, while numbers (parts a, b, c) identify data points. Data sources: Harris County Flood Control District (2022b); TranStar (2022).

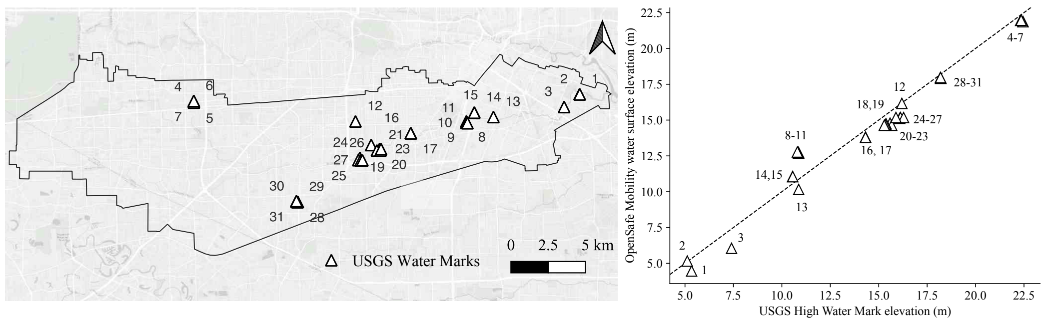

Figure 11: Comparison of observed USGS high water level marks with OpenSafe Mobility model predictions for Hurricane Harvey. Numbers locate data points on the map. Data sources: U.S. Geological Survey (2022a); Harris County Flood Control District (2022b).

$e_j = A_j - P_j$, A_j is the observed value, P_j is the model predicted value, and n is the number of observations. Similarly, mean absolute error (MAE) is defined as $1/n \sum_{j=1}^{n} |e_j|$ and root mean square error (RMSE) is defined as $\sqrt{1/n \sum_{j=1}^{n} e_j^2}$. It can also be noted that OpenSafe Mobility model predictions slightly underestimate flood depths. Further, visual inspection of the data indicates that the model predictions are within the observed range of values for 7 out of 10 flood observations. Similarly, Fig. 11 plots the USGS High Water Level Marks (HWLMs) with water surface elevation from OpenSafe Mobility. Comparison results (ME=0.21, MAE=0.77, RMSE=0.93 for 31 observations) indicate a similar model performance as the camera data. These results show that OpenSafe Mobility can provide flood depth estimates with reasonable accuracy and identify flooded roads.

In both Imelda and Beta, no widespread flooding was observed in the study region. For TS Imelda (ME=-0.27, MAE=0.27, RMSE=0.68 for 6 observations), the model ($M2$) correctly predicts all cases except one (Fig. 10-b (point 12)), where OpenSafe Mobility overestimates the flood depth on a portion of Interstate-69 that is flanked by elevated embankments, resulting in a deep, channel-like topography. This error demonstrates the model's inability to account for artificial drainage systems. Likewise for TS Beta, OpenSafe Mobility ($M2$) overestimated flood depth at three locations along the SH288 highway as demonstrated by the results (ME=-0.09, MAE=0.30, RMSE=0.38 for 6 observations). This may be due to the fact that for small events such as Imelda and Beta, storm networks are effective in reducing the intensity of flooding. Since OpenSafe Mobility cannot currently model storm networks, it overestimates the flood depth. Despite these limitations, OpenSafe Mobility provided flood depth estimates with reasonable accuracy for most locations tested. Further, locations where the model will fail are predictable based on the topography.

3.6. An Overview of OpenSafe Mobility Results for Hurricane Harvey

This section evaluates OpenSafe Mobility's capacity to identify flooded roads and contrasts it to the Texas Department of Transportation (TxDOT) flood closure reports. Further, it also demonstrates OpenSafe Mobility's ability to quantify link and network-level flood impacts considering vehicle characteristics and roadway topography. This validation exercise is limited to the Hurricane Harvey case study since only Hurricane Harvey had any notable network-wide impact on roads in the study region. Fig. 12-1a locates all flood reports from TxDOT (Texas Department of Transportation, 2022) in the study region during Hurricane Harvey. Similarly, Fig. 12-1b-e show the temporal evolution of flooding using closure reports from TxDOT. A closer examination of the TxDOT data reveals that all closed roads are not flooded. The TxDOT data, for example, shows that the whole Interstate-610 loop around Houston is closed due to floods. While portions of Interstate-610 were flooded, the loop as a whole was not flooded but was closed to the public. As a result, a direct comparison of TxDOT data with OpenSafe Mobility reports may not be fully appropriate; however the comparison is made herein for insights on roadway level performance.

Fig. 12-2a-e show flood reports from OpenSafe Mobility for passenger cars. For identifying flooded roads, see the methodology described in Section 2.3. For Fig. 12-2a-i, a wading height of 0.5 m is used to identify roads flooded for passenger cars. Fig. 12-2a shows the collection of all roads impacted at any time during Harvey. Comparing Fig. 12-2a with Fig. 12-1a highlights the increase in data availability using OpenSafe Mobility compared to TxDOT. Fig. 12-2b-e show the evolution of roadway flooding at different time steps during Harvey. Further, Fig. 12-2f-i show the evolution of access to hospitals quantified using connectivity loss (CL) ratio. CL ratio is estimated by performing network analysis on the updated network without flooded roads at any time step. The regions with severe connective loss might have limited access to hospitals using passenger cars with wading height 0.5m or less.

Similarly, Fig. 12-3a-i show the road condition and network-level impacts for high water vehicles. Here, a 1.2 m (4 ft) wading height is used to identify flooded roads and quantify network-level impacts. It is important to notice that many roads flooded for passenger cars are open for high water trucks; consequently, many regions inaccessible via a passenger car are accessible to high water trucks. This illustrates the importance of considering vehicle characteristics while identifying flood impacts. Furthermore, sites inaccessi-

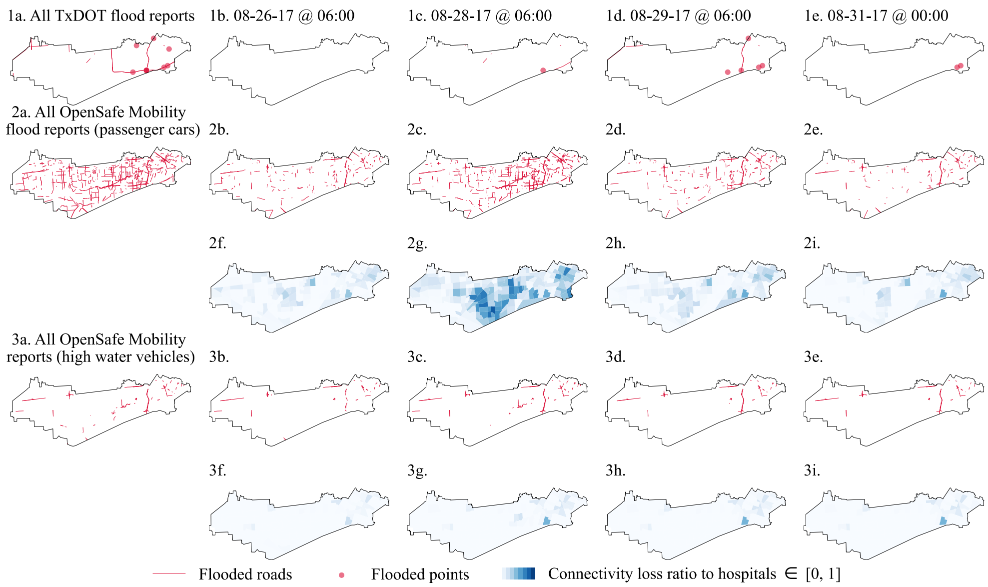

Figure 12: Comparison of flood observations from TxDOT and results from OpenSafe Mobility at various time steps. OpenSafe Mobility can provide vehicle class-specific road trafficability data as well as assess the accessibility to select facilities. A depth-centric approach is used here to identify flooded roads. A road is considered closed for a vehicle if the water depth over the road exceeds the safe wading height. A safe wading height of 0.5 m is considered for passenger cars (parts 2a-i) and 1.2m for high-water vehicles (3a-i). The first column reports flooded roads at any time during Hurricane Harvey, and the remaining columns represent conditions at select time steps indicated in the first row (parts 1b-e). Data sources: Texas Department of Transportation (2022), Harris County Flood Control District (2022b), and OpenStreetMap contributors (2017).

ble to high-water trucks necessitate specialized equipment, such as boats, to carry out any emergency response operation.

Fig. 13-a-i illustrate a probabilistic approach to quantify flood impact on roads. Here, a normal distribution ($\mathcal{N}(0.4125\text{m}, 0.0232\text{m})$)(Contreras-Jara et al., 2018) is used to model the wading height of passenger cars. Given flood depths at roads, the probability of a road being impassable is the probability of wading height less than the flood depth. Fig. 13-a depicts the maximum probability of roads being impassable at any time throughout the storm. Fig. 13-b-e show the temporal evolution of the probability of roads being impassable for the select vehicle class. The probability of road closure data will aid decision-makers in deciding road closure decisions and managing risk. For example, a traffic information system can tag any roads with a probability of flooding greater than a threshold, such as 5%, as flooded. Further, emergency responders can identify flooded roads and inaccessible regions based on risk tolerance and available equipment. For example, Fig. 13-f-i show access to hospitals considering only roads with a 95% probability of remaining open.

Fig. 14-1a-i and Fig. 14-2a-i illustrate the stability-centric approach to identify flooded roads. Fig. 14-1a and 2a show any road that experienced unsafe conditions for small passenger cars and large 4WD vehicles following AR&R criteria. Fig. 14-1b-e and Fig. 14-2b-e identify unsafe roads, and Fig. 14-1f-i and Fig. 14-2f-i quantify network level impacts of road closures on access to hospitals for small passenger and large 4WD vehicles respectively.

These validation case studies showcased the capacity of OpenSafe Mobility to provide reliable estimates of link and network-level impacts of flood-

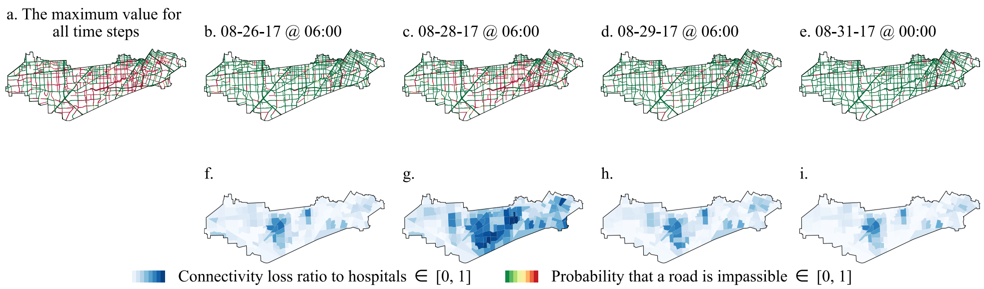

Figure 13: The probabilistic depth-centric approach for estimating road link conditions and network-level impacts of flooding. Here, a wading height distribution for passenger cars and water depth over roads are used to infer the probability of road links being impassable (parts a-e). Access to hospitals (parts f-i) is then evaluated only considering road links with a 95% probability of remaining open. The first column depicts the maximum probability of roads being impassable at any time during Hurricane Harvey, and the remaining columns represent conditions at select time steps indicated in the first row (parts b-e). Data sources: Harris County Flood Control District (2022b) and OpenStreetMap contributors (2017).

ing. OpenSafe Mobility significantly advances the state-of-the-art situational awareness frameworks focused on mobility. Continued validation can occur as data is collected and the framework is tested in an online deployment.

4. Deployment

A prototype of the OpenSafe Mobility framework has been operational since 8 Sept 2021. In this limited deployment, OpenSafe Mobility is run on a local workstation (Intel Core i7-4790 CPU @3.60 GHz and 16 GB RAM). Python packages are used to process radar rainfall (Basyal, 2022), automate HEC-RAS runs (Dysarz, 2018), perform network (Hagberg et al., 2008) and spatial analyses (Jordahl et al., 2020). The M3 version of the model is used with gauge-adjusted radar rainfall data from Vieux & Associates, Inc. The

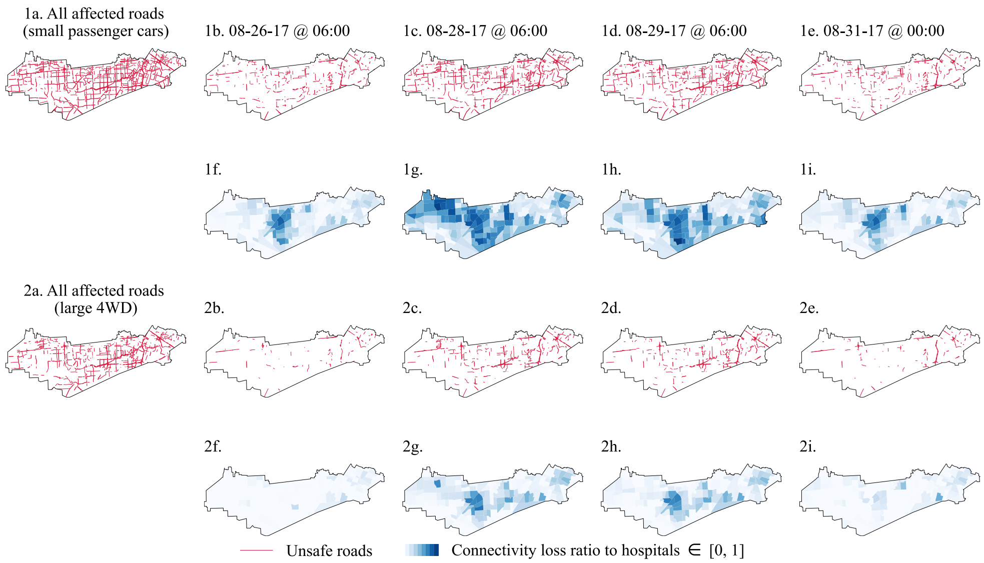

Figure 14: The stability-centric approach for estimating road link conditions and network-level impacts of flooding. Here, AR&R stability criteria are used to identify unsafe roads for small passenger cars (parts 1a-e) and large 4WD vehicles (parts 2a-e). Access to hospitals is then evaluated only considering safe roads for small passenger cars (parts 1f-i) and large 4WD vehicles (parts 2f-i). The first column reports unsafe road links at any time during Hurricane Harvey, and the remaining columns represent conditions at select time steps indicated in the first row (parts 1b-e). Data sources: Texas Department of Transportation (2022), Harris County Flood Control District (2022b), OpenStreetMap contributors (2017), and U.S. Department of Homeland Security (2022).

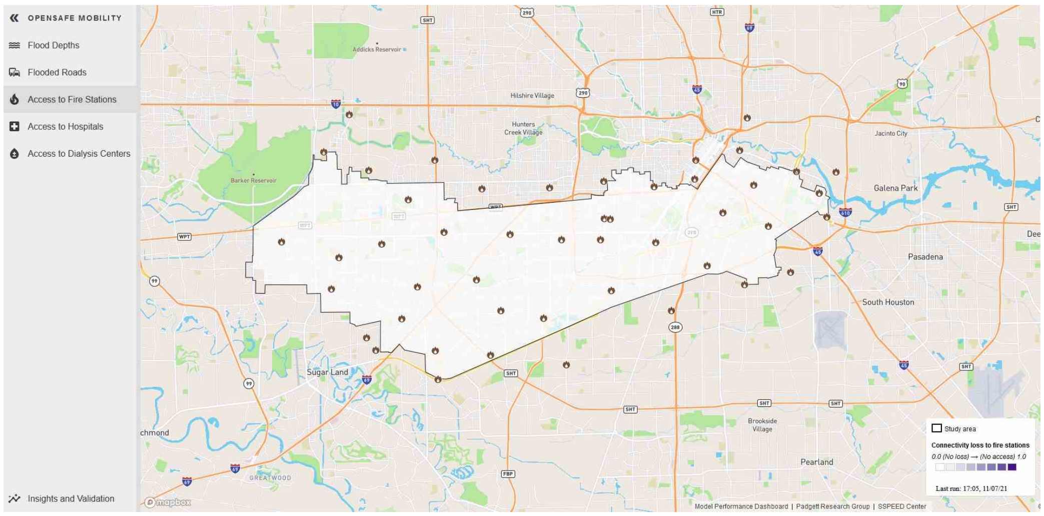

Figure 15: Screenshot of the OpenSafe Mobility website.

preceding eight days of rainfall data (d_{max} = 8 days) are used to model current flood conditions at each time step. The results are then uploaded to Amazon Simple Storage Service. Finally, the results are published using a website developed using HTML, JavaScript, CSS, and Mapbox. Currently, the OpenSafe Mobility website (Fig. 15) is hosted on Amazon Web Services and can be accessed at www.opensafemobility.com. The typical time lag is between 10 and 28 minutes, which includes the time it takes to acquire (5-18 minutes) and process the gage-adjusted radar data ($<$ 1min), run the flood model (2-10 minutes), perform network and spatial analysis (3-4 minutes), and publish the results ($<$ 1 min).

Since the model's deployment, no major flood events have occurred in the study region. As a result, the model's performance cannot be assessed further at this point. However, for reliable stakeholder dependent deployment two limitations of the system architecture should be addressed in the long term. These include the need for hosting on multiple computers that are not co-located with the study region. Additionally, future deployments would ideally leverage multiple data sources, as the current system relies on a single radar data source.

5. Discussion

5.1. OpenSafe Mobility Framework and Case Studies

This paper proposed a new situational awareness framework for nowcasting road network conditions during flooding. It combined a state-of-the-art flood model, widely available gage-adjusted radar rainfall data, and network and spatial analyses using open-source tools and data to infer vehicle-class specific road conditions and community access. A case study analysis then evaluated the nowcasting model for Brays Bayou Watershed in Houston, Texas. The case study used four recent storms in the watershed and tested the ability of OpenSafe Mobility to sense the flooding using quantitative and qualitative metrics.

Finally, it is essential to note that OpenSafe Mobility does not identify flooded roads to facilitate routing over flooded streets. Instead, it seeks to identify open roads to support routing, reduce delays and detours, and enhance roadway safety. It also aims to support decision-making by identifying affected regions and aiding emergency response vehicle selection to access isolated neighborhoods. While limitations certainly exist in the flood depth predictions due to the numerical nature of the hydraulic model and uncertainties associated with modeling large storm events, the validation exercises prove that OpenSafe Mobility can sense flood impact on road networks and aid in identifying open roads for emergency vehicles.

5.2. Assumptions and Limitations

Case studies highlight several limitations of the OpenSafe Mobility framework. HEC-RAS 6.0, and consequently OpenSafe Mobility, cannot model the underground drainage network and as such, pluvial flooding is overestimated. However, because Houston's drainage network is only designed to handle a 2-year storm (Haddock and Kanwar, 2021)(50% annual chance), and because OpenSafe Mobility is only triggered with a higher threshold event (say 5-year event or greater), the overestimation of flood extents is limited. During large storm events, the drainage system is overwhelmed and therefore the assumption made in this methodology is reasonable that the runoff will mostly remain overland and not be funneled into culverts and underground pipes. The lack of underground drainage modeling can also lead to an underestimation of fluvial flooding, as water that is normally routed into bayous via underground networks are not being modeled. Therefore, a more accurate model would be able to account for underground drainage, either by deducting a 2-year rainfall from the input rainfall, or by using a model that accounts for underground drainage (BMT Commercial Australia Pty Ltd, 2022) (although the latter can be infeasible and time-consuming for watershed-scale modeling).

Additionally, pumping systems that play a critical role in pumping water out of low spots on freeways were not modeled. This was due to a lack of information about these pumps (such as flow rate) as well as the modeling difficulties that arise when pumps are introduced (such as model instability). Because of this, OpenSafe Mobility displays flooding at freeway underpasses that otherwise may have been pumped out. Like the underground drainage system, these pumps can be overwhelmed in large storms events, which makes our lack of pumps a reasonable assumption. However, as seen with the validation and calibration results, a model that performs well for a longer duration storm event (such as Hurricane Harvey) may not perform as well for a shorter storm event (such as TS Beta). Additionally, a model that performs well for a single-peak event (such as the Tax Day flooding) did not perform as well for the triple-peak event of TS Imelda. To account for this variability, future versions of OpenSafe Mobility could consider deploying different models depending on storm characteristics.

5.3. Transferability and Scalability

OpenSafe Mobility might be transferrable to other regions for which reliable data is available for replicating the framework. Data needs and example data sources for OpenSafe Mobility are listed in Table 1. Rainfall data sources that can be used in OpenSafe Mobility, whether rain gage data or radar data, are widely available. Some examples are NEXRAD (for the US) and Operational Programme for the Exchange of Weather Radar Information (for Europe). Further, several existing methodologies and open source tools exist in the literature to facilitate fusion of gage data and radar data to generate GARR. While the case studies presented in the paper only used GARR to validate OpenSafe Mobility performance, rain gage or radar data could also be used. Since the accuracy of rainfall data will affect the reliability of OpenSafe Mobility results, any future deployment should test model performance using the adopted rainfall source(s). Other data required for flood modeling, such as the terrain, land cover data, imperviousness data, and bathymetry data, are widely available and commonly used in hydrologic and hydraulic models. Similarly, data for network and spatial analyses can be obtained from OpenStreetMaps and the census department. For deployment, the OpenSafe Mobility web framework uses HTML, CSS, JavaScript, and Mapbox. While Mapbox is not open source, similar functionality can be replicated using Leaflet—an open-source JavaScript library. All codes required to implement the OpenSafe Mobility are available in the project's GitHub repository (Panakkal et al., 2022). OpenSafe Mobility may be transferable to communities with access to hydrologic and hydraulic models and reliable input data (Table 1); however, significant investments may be required for areas without access to accurate data and models.

5.4. Future Opportunities

OpenSafe Mobility provides a deterministic prediction of flooding. Flooding involves complex interactions between the built environment and water, and a probabilistic model may be better suited to provide a holistic representation of flood hazards. Running a suite of flood models instead of a single model used in OpenSafe Mobility can effectively provide a probability measure of flood hazard, albeit engendering considerable computation and processing costs. Surrogate models based on deep learning that can leverage GPUs offer a promising approach to enable real-time probabilistic flood inundation mapping. OpenSafe Mobility can be further improved by augmenting it with other data sources such as traffic cameras and official traffic alerts. For example, traffic cameras overlooking potential ponding locations can be used to adjust OpenSafe Mobility predictions and correct for overestimation of flooding in such regions. Further, OpenSafe Mobility doesn't currently attempt to forecast road conditions; instead, it's designed to detect current flood conditions on the road after rainfall has occurred within an acceptable time lag. Recent advances in radar nowcasting (Ravuri et al., 2021) can be used in the future to forecast road conditions. Future studies should also test the transferability and scalability of the OpenSafe Mobility framework to different regions with diverse topography, situational awareness needs, and data availability. Finally, the current version of OpenSafe Mobility did not consider systemic stakeholder needs assessment and instead concentrated on methodological aspects; future versions and deployments of OpenSafe Mobility should be co-developed with stakeholders following the tenets of user-centered design principles (Robinson et al., 2005).

5.5. Key Contributions in the Context of Existing Frameworks

OpenSafe Mobility advances the current state-of-the-art by providing vehicle-specific road condition and network impact data at high spatial and temporal resolution and with limited time lag and bias compared to most existing situational awareness tools. Similar to frameworks leveraging physical water level sensors, OpenSafe Mobility can provide inundation depth to support decision making considering vehicle characteristics. Although less accurate than water level sensors, the low cost and high availability coupled with an acceptable accuracy make OpenSafe Mobility a good candidate to complement depth sensors. Ideally such sensors should be sited in regions where the accuracy of OpenSafe Mobility is limited. Further, OpenSafe Mobility provides a competent alternative to social sensors; especially, it provides a source devoid of biases in social sensors, provides quantitative flood depth estimates, and can match or exceed the availability of social sensors.

When compared to remote sensors (e.g., satellite images, UAVs), OpenSafe Mobility provides quantitative water depth estimates with limited time lag and is not affected by factors such as cloud or vegetation cover.

Next, OpenSafe Mobility enables equitable access to situational awareness data for flood-prone communities. Flood-prone communities with access to data and models required for OpenSafe Mobility can leverage the framework to aid decision-making and situational awareness, making it a sustainable, low-cost alternative to costly options such as physical sensors.

Finally, this study advances the current state-of-the-art for using flood models to infer flood impacts on roads in real time. Specifically, the results show that a multi-disciplinary approach integrating radar rainfall data, physics-based flood models, vehicle characteristics, roadway topography, and network and spatial analyses can provide high-resolution information on flood impact on transportation networks. The proposed framework distinguishes itself from the existing flood model-based frameworks (Panakkal et al., 2019; Mioc et al., 2015; Ming et al., 2020; Naulin et al., 2013; Versini et al., 2010; Morsy et al., 2018) in terms of its focus on roadway mobility (especially in terms of vehicle-specific road link- and network-level impacts), consideration of flood mechanism (enabling it to infer the conditions of roads away from the streams), roadway topography (allowing it to capture roadway elevation), and vehicle stability. Further, the study highlighted the limitations of the proposed model and suggested future work to address them.

6. Conclusions

Reliable nowcasting of roadway conditions during flooding is a long-standing challenge with societal importance for emergency response and roadway safety. Our approach using radar rainfall data and a physics-based flood model directly addresses this vital problem and provides current information on connectivity to critical facilities. We showed using case studies that the proposed framework offers improved nowcasting of roadway conditions. Primarily, it can provide high-resolution data on local roads and vehicle class-specific road condition data needed for vehicle and route selection for emergency response. The real-time convergence of flood estimation with the vehicle-specific link- and network-level analyses distinguishes OpenSafe Mobility as a unique mobility-centric framework that addresses the growing need to sense road conditions during flooding. Further, while not attempted in this paper, the proposed framework might be transferable to other regions with access to reliable hydrologic and hydraulic models and real-time rainfall data. Any implementation of OpenSafe Mobility should be tailored to the data availability in the study region and undergo extensive testing before widespread adoption. While continued development and extensive testing under diverse storms and data availability are still required, OpenSafe Mobility has the potential to augment existing ITS tools and equip emergency managers and responders with a holistic picture of flood impact on mobility and community access.

Yet, there remain further challenges to be addressed in our nowcasting framework. As case studies demonstrated, OpenSafe Mobility provides reliable flood impact prediction during major floods, but modeling the impact of stormwater networks and pumping stations remains difficult. Critically, OpenSafe Mobility could overestimate flooding in regions with efficient artificial drainage systems. Future versions of OpenSafe Mobility will address this challenge by integrating stormwater networks in hydraulic and hydrologic models and leveraging information from other sources such as traffic cameras using data fusion. Another important challenge not discussed in this study is the scalability of the model to a large area. Implementing a model for a large urban area such as Greater Houston could increase model delay from under 30 minutes to over an hour. Such a high time lag is undesirable for situational awareness applications. Using a surrogate model to capture hydrological and hydraulic models as an alternative to the physics-based flood model could reduce the time lag. Further, real-time network analysis for a large network requires leveraging recent developments in surrogate models (Stern et al., 2017) and network analysis (Leskovec and Sosič, 2016). Finally, OpenSafe Mobility uses a deterministic model to capture flooding; given the complexity of the flooding process, a probabilistic approach can be leveraged to account for uncertainties. Despite these shortcomings, OpenSafe Mobility provides a pathway to reliable situational awareness for communities.

Acknowledgments

This work was supported by the National Science Foundation (NSF) award numbers 1951821, 1842494, and 1545837. Authors would like to acknowledge the contributions of David Brooks (support with access to radar data), Matthew Garcia (guidance on flood modeling), Joe Hurley and Steven Michalek (support with access to TxDOT public data), and Rice University

GIS/Data Center (support with access to LiDAR open data). The authors thank the anonymous reviewers for their constructive feedback. Any opinions, findings, and conclusions or recommendations expressed in this paper are those of the authors and do not necessarily reflect the views of the sponsors.

Appendix A. Model Performance for Fluvial Flooding

Fluvial validations are achieved by comparing observed and modeled temporal water surface elevations (WSE) at three United States Geological Survey (USGS) gages along Brays. By visual inspection, a good validation is one that agrees well with observed data in both the peak and timing of the stage hydrograph. Quantitatively, validations are measured by the Nash-Sutcliffe Efficiency index (NSE) (Nash and Sutcliffe, 1970). NSE values range between $-\infty$ and 1, with 1 being an exact match to observed data, and negative values indicating that the average of the observed data would be a better fit than the modeled data.

As can be seen in Fig. A.16e-f, the model demonstrates a good fit qualitatively (hydrograph timing and peak) for gages at Gessner Dr. and Main St. For the most upstream gage, Brays at Alief (Fig. A.16d), the model underestimates peak WSE in the validation case despite a good match in hydrograph timing. However, the authors determined that this was a satisfactory validation as most flooding in the watershed occurs further downstream than this gage, and the gages further downstream displayed good model performance.

Further validation exercises continued to prove the validity of the model. As shown in Fig. A.17j-l, the model validation of Tropical Storm Beta

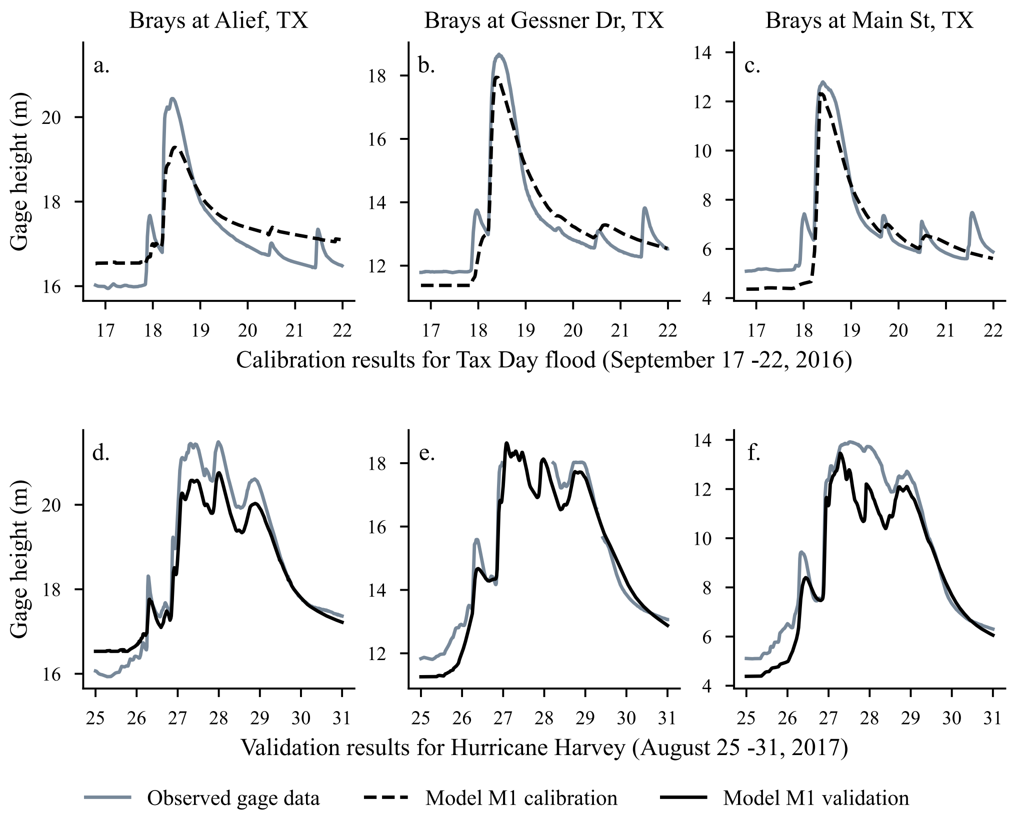

Figure A.16: Observed and predicted gage heights at three watchpoints along Brays Bayou. Model $M1$ was calibrated on Tax Day flood (part a-c) and validated on Hurricane Harvey (part d-f). The results show good agreement between model prediction and observed rainfall during validation (part d-f). The broken line in part e indicates no data due to gage malfunction. Data source: U.S. Geological Survey (2022b).

matched in both hydrograph peak and timing. The validation of Tropical Storm Imelda (Fig. A.17g-i) contained discrepancies in the falling limbs of the hydrographs, however, for this tri-peak storm, the timings and values of peak WSEs were well-matched. The errors in the falling limb of this validation lead only to a conservative estimation of flooding by predicting a prolonged flooding. Therefore, the authors concluded a satisfactory validation of $M2$. Model $M3$ is validated on all four storms. The red dotted lines in Fig. A.17a-l display the $M3$ calibration, which is the final calibration version of the model used in the deployment of OpenSafe Mobility. Overall, and especially for the two downstream gages of Gessner Dr. and Main St., the model shows a satisfactory match to observed stage data.

The accuracy of a model can also be quantitatively measured using the NSE index. As the four validations storms were quite different in duration, intensities, total rainfall, and temporal patterns, it was a challenge to create a model that was robust in its applicability to various types of storms. However, using $M3$, which was calibrated using all four historical storms, the NSE values for all storms and at all gages are satisfactory, as shown in Table A.2. Notably, the gage at Gessner Dr. has good validations for all storms, which is important for this work as most flooding is observed in the area around this gage (the Meyerland area). Due to the good qualitative and quantitative validations of the model, it was adopted for predicting flood levels in OpenSafe Mobility.

Ahmad, K., Pogorelov, K., Riegler, M., Ostroukhova, O., Halvorsen, P., Conci, N., Dahyot, R., 2019. Automatic detection of passable roads after

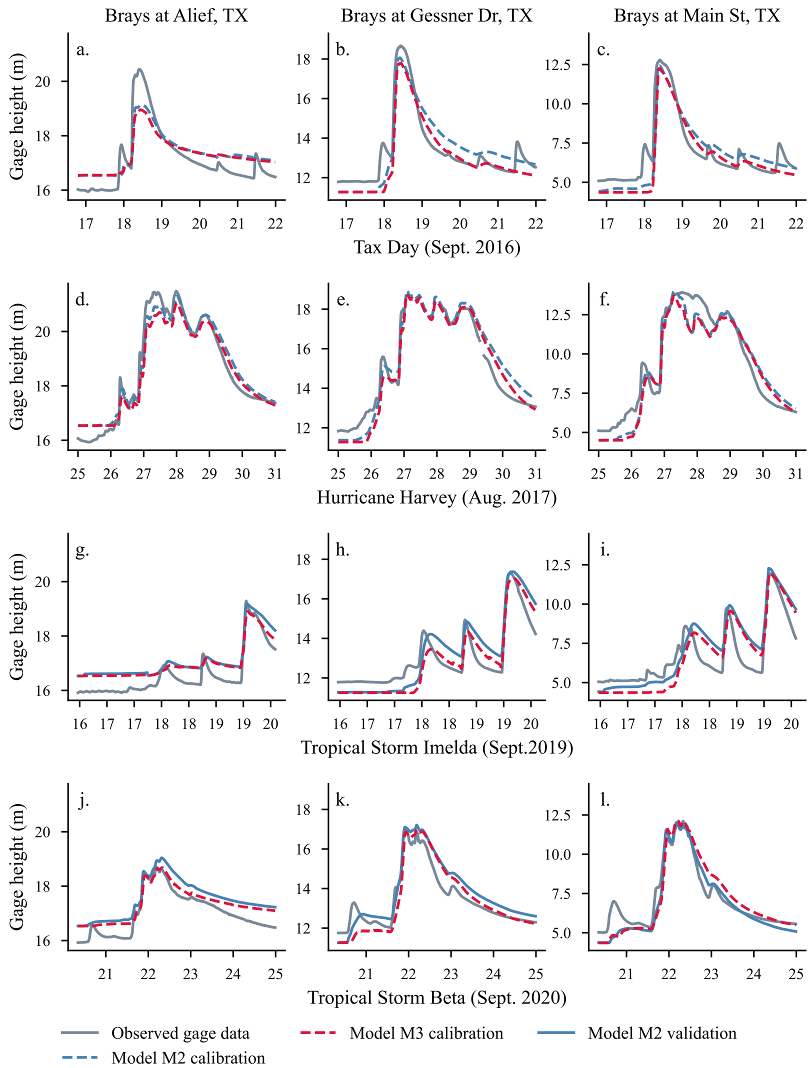

Figure A.17: Observed and predicted gage heights at three watchpoints along Brays Bayou for four case study storms. Model $M2$ was calibrated on Tax Day flood (part a-c) and Hurricane Harvey (part d-f) and validated on Tropical Storms Imelda (part g-i) and Beta (part j-l). Similarly, Model $M3$ was calibrated on all four storms. During the validation stage, Model $M2$ showed acceptable performance for unseen storms. Data source:U.S. Geological Survey (2022b).

Table A.2: Summary of model performance

Model	Gage	NashSutcliffe model efficiency coefficient[1]			
		Tax Day	Harvey	Imelda	Beta
$M1$	Alief	0.80	**0.92**		
	Gessner Dr.	0.95	**0.93**		
	Main St.	0.93	**0.88**		
$M2$	Alief	0.79	0.96	**0.60**	**0.53**
	Gessner Dr.	0.92	0.87	**0.70**	**0.82**
	Main St.	0.92	0.91	**0.64**	**0.89**
$M3$	Alief	0.75	0.94	0.68	0.76
	Gessner Dr.	0.93	0.89	0.79	0.82
	Main St.	0.91	0.90	0.63	0.83

[1] The results in normal font are calibration results and the results in the bold font are validation results. For example, Model $M1$ was calibrated using Tax Day flood and validated on Hurricane Harvey. Similarly, Model $M2$ was calibrated using Tax Day, Hurricane Harvey and validated on Tropical Storms Imelda and Beta.

floods in remote sensed and social media data. Signal Processing: Image Communication 74, 110–118. doi:10.1016/j.image.2019.02.002.

Basyal, G., 2022. Pydsstools. URL: https://github.com/gyanz/pydsstools. (Last Accessed: 2022-03-06).

Beven, J.L., Berg, R., 2021. Tropical Cyclone Report Tropical Storm Beta (AL222020) 1722 September 2020. Technical Report. National Hurricane Center.

Blake, E., Zelinsky, D., 2018. Tropical Cyclone Report Hurricane Harvey (AL092017) 17 August 1 September 2017. Technical Report. National Hurricane Center.

BMT Commercial Australia Pty Ltd, 2022. TUFLOW. URL: https://www.tuflow.com/. (Last Accessed: 2022-01-04).

Bocanegra, R.A., Valls-Morn, F.J., Francs, F., 2020. Review and analysis of vehicle stability models during floods and proposal for future improvements. Journal of Flood Risk Management 13, e12551. URL: https://onlinelibrary.wiley.com/doi/abs/10.1111/jfr3.12551, doi:10.1111/jfr3.12551. _eprint: https://onlinelibrary.wiley.com/doi/pdf/10.1111/jfr3.12551.

Botchkarev, A., 2019. Performance Metrics (Error Measures) in Machine Learning Regression, Forecasting and Prognostics: Properties and Typology. Interdisciplinary Journal of Information, Knowledge, and Management 14, 045–076. URL: http://arxiv.org/abs/1809.03006, doi:10.28945/4184. arXiv: 1809.03006.

Brunner, G.W., 2021. HEC-RAS River Analysis System 2D Modeling User's Manual Version 6.0 Beta. Technical Report CPD-68A. USACE Hydrologic Engineering Center: Davis, CA, USA.

Carreño Conde, F., De Mata Muñoz, M., 2019. Flood monitoring based on the study of sentinel-1 sar images: The ebro river case study. Water 11, 2454.

Chakraborty, J., Collins, T.W., Grineski, S.E., 2019. Exploring the Environmental Justice Implications of Hurricane Harvey Flooding in Greater Houston, Texas. American Journal of Public Health 109, 244–250. doi:10.2105/AJPH.2018.304846. publisher: American Public Health Association.

Chaudhary, P., DAronco, S., Moy de Vitry, M., Leito, J.P., Wegner, J.D., 2019. Flood-Water Level Estimation from Social Media Images. ISPRS Annals of the Photogrammetry, Remote Sensing and Spatial Information Sciences IV-2/W5, 5–12. doi:10.5194/isprs-annals-IV-2-W5-5-2019.

City of Houston, 2022. Houston, Texas 3-1-1. URL: https://www.houstontx.gov/311/. (Last Accessed: 2022-03-27).

Coles, D., Yu, D., Wilby, R.L., Green, D., Herring, Z., 2017. Beyond flood hotspots: Modelling emergency service accessibility during flooding in York, UK. Journal of Hydrology 546, 419–436. URL: https://www.sciencedirect.com/science/article/pii/S0022169416308022, doi:10.1016/j.jhydrol.2016.12.013.

Contreras-Jara, M., Echaveguren, T., Vargas Baecheler, J., Chamorro Gin, A., de Solminihac Tampier, H., 2018. Reliability-Based Estimation of Traffic Interruption Probability due to Road Waterlogging. Journal of Advanced Transportation 2018, e2850546. doi:10.1155/2018/2850546. publisher: Hindawi.

Dao, D.A., Kim, D., Kim, S., Park, J., 2020. Determination of flood-inducing rainfall and runoff for highly urbanized area based on high-resolution radar-gauge composite rainfall data and flooded area GIS data. Journal of Hydrology 584, 124704. doi:10.1016/j.jhydrol.2020.124704.

De Longueville, B., Smith, R.S., Luraschi, G., 2009. " OMG, from here, I can see the flames!" a use case of mining location based social networks to acquire spatio-temporal data on forest fires, in: Proceedings of the 2009 international workshop on location based social networks, pp. 73–80.

Dey, K.C., Mishra, A., Chowdhury, M., 2015. Potential of Intelligent Transportation Systems in Mitigating Adverse Weather Impacts on Road Mobility: A Review. IEEE Transactions on Intelligent Transportation Systems 16, 1107–1119. doi:10.1109/TITS.2014.2371455.

Dijkstra, E.W., 1959. A note on two problems in connexion with graphs. Numerische Mathematik .

Dysarz, T., 2018. Application of Python Scripting Techniques for Control and Automation of HEC-RAS Simulations. Water 10, 1382. doi:10.3390/w10101382.

Esri, 2022. Esri World Light Gray Base Map. URL: http://services.arcgisonline.com/ArcGIS/rest/services/Canvas/World_Light_Gray_Base/MapServer/tile/%7Bz%7D/%7By%7D/%7Bx%7D. (Last Accessed: 2022-03-27).

Evans, B., Chen, A.S., Djordjevi, S., Webber, J., Gmez, A.G., Stevens, J., 2020. Investigating the Effects of Pluvial Flooding and Climate Change on Traffic Flows in Barcelona and Bristol. Sustainability 12, 2330. URL: https://www.mdpi.com/2071-1050/12/6/2330, doi:10.3390/su12062330. number: 6 Publisher: Multidisciplinary Digital Publishing Institute.

Fan, C., Esparza, M., Dargin, J., Wu, F., Oztekin, B., Mostafavi, A., 2020a. Spatial biases in crowdsourced data: Social media content attention concentrates on populous areas in disasters. Computers, Environment and Urban Systems 83, 101514. Publisher: Elsevier.

Fan, C., Wu, F., Mostafavi, A., 2020b. A Hybrid Machine Learning Pipeline for Automated Mapping of Events and Locations From Social Media in Disasters. IEEE Access 8, 10478–10490. doi:10.1109/ACCESS.2020.2965550. conference Name: IEEE Access.

Fang, Z., Bedient, P.B., Buzcu-Guven, B., 2011. Long-Term Performance of a Flood Alert System and Upgrade to FAS3: A Houston, Texas, Case Study. Journal of Hydrologic Engineering 16, 818–828. doi:10.1061/(ASCE)HE.1943-5584.0000374. publisher: American Society of Civil Engineers.

Fang, Z., Dolan, G., Sebastian, A., Bedient, P.B., 2014. Case Study of Flood

Mitigation and Hazard Management at the Texas Medical Center in the Wake of Tropical Storm Allison in 2001. Natural Hazards Review 15, 05014001. doi:10.1061/(ASCE)NH.1527-6996.0000139. publisher: American Society of Civil Engineers.

Faturechi, R., Miller-Hooks, E., 2015. Measuring the Performance of Transportation Infrastructure Systems in Disasters: A Comprehensive Review. Journal of Infrastructure Systems 21, 04014025. doi:10.1061/(ASCE)IS.1943-555X.0000212. publisher: American Society of Civil Engineers.

FEMA, 2022. FEMA Flood Map Service Center. URL: https://msc.fema.gov/portal/home. (Last Accessed: 2022-03-27).

Field, C.B., Barros, V., Stocker, T.F., Dahe, Q., 2012. Managing the risks of extreme events and disasters to advance climate change adaptation: special report of the intergovernmental panel on climate change. Cambridge University Press.

Geetha, M., Manoj, M., Sarika, A.S., Mohan, M., Rao, S.N., 2017. Detection and estimation of the extent of flood from crowd sourced images, in: 2017 International Conference on Communication and Signal Processing (ICCSP), IEEE. pp. 0603–0608.

Google LLC, 2022a. Driving directions, live traffic & road conditions updates. URL: https://www.waze.com/live-map/. (Last Accessed: 2022-03-18).

Google LLC, 2022b. Material Icons Guide | Google Fonts. URL: https://developers.google.com/fonts/docs/material_icons. accessed August 25, 2022.

Gori, A., Gidaris, I., Elliott, J.R., Padgett, J., Loughran, K., Bedient, P., Panakkal, P., Juan, A., 2020. Accessibility and Recovery Assessment of Houstons Roadway Network due to Fluvial Flooding during Hurricane Harvey. Natural Hazards Review 21, 04020005. doi:10.1061/(ASCE)NH.1527-6996.0000355. publisher: American Society of Civil Engineers.

Green, D., Yu, D., Pattison, I., Wilby, R., Bosher, L., Patel, R., Thompson, P., Trowell, K., Draycon, J., Halse, M., Yang, L., Ryley, T., 2017. City-scale accessibility of emergency responders operating during flood events. Natural Hazards and Earth System Sciences 17, 1–16. URL: https://nhess.copernicus.org/articles/17/1/2017/, doi:10.5194/nhess-17-1-2017. publisher: Copernicus GmbH.

Guerrero-Ibez, J., Zeadally, S., Contreras-Castillo, J., 2018. Sensor Technologies for Intelligent Transportation Systems. Sensors 18, 1212. doi:10.3390/s18041212.

Hackl, J., Lam, J.C., Heitzler, M., Adey, B.T., Hurni, L., 2018. Estimating network related risks: A methodology and an application in the transport sector. Natural Hazards and Earth System Sciences 18, 2273–2293. URL: https://nhess.copernicus.org/articles/18/2273/2018/, doi:10.5194/nhess-18-2273-2018. publisher: Copernicus GmbH.

Haddock, C., Kanwar, S., 2021. Infrastructure Design Manual 2021. Technical Report. City of Houston, Houston Public Works. Houston. URL: https://parkusa.com/index.php/files/132/SW-Harris-County---COH/384/COH-Infrastructure-Design-Manual.pdf.

Hagberg, A., Swart, P., S Chult, D., 2008. Exploring network structure, dynamics, and function using NetworkX. Technical Report. Los Alamos National Lab.(LANL), Los Alamos, NM (United States).

Han, Z., Sharif, H.O., 2021. Analysis of Flood Fatalities in the United States, 19592019. Water 13, 1871. doi:10.3390/w13131871. number: 13 Publisher: Multidisciplinary Digital Publishing Institute.

Harris County Flood Control District, 2022a. Harris County Flood Warning System. URL: https://www.harriscountyfws.org/. (Last Accessed: 2022-03-18).

Harris County Flood Control District, 2022b. Model and Map Management (M3) System. URL: https://www.hcfcd.org/Resources/Interactive-Mapping-Tools/Model-and-Map-Management-M3-System. (Last Accessed: 2022-03-04).

Harris County Flood Control District, 2022c. Project Brays Features. URL: https://www.hcfcd.org/Activity/Active-Projects/Brays-Bayou/C-11-Project-Brays/Project-Brays-Features. (Last Accessed: 2022-03-04).

He, X., Lu, D., Margolin, D., Wang, M., Idrissi, S.E., Lin, Y.R., 2017. The signals and noise: actionable information in improvised social media channels during a disaster, in: Proceedings of the 2017 ACM on web science conference, pp. 33–42.

Houston-Galveston Area Council, 2022. LiDAR Imagery | Houston-

Galveston Area Council (H-GAC). URL: https://www.h-gac.com/imagery/lidar. (Last Accessed: 2022-03-04).

Iowa State University, 2022. MRMS data archive. URL: https://mtarchive.geol.iastate.edu/. (Last Accessed: 2022-03-06).

Jiang, J., Liu, J., Qin, C.Z., Wang, D., 2018. Extraction of Urban Waterlogging Depth from Video Images Using Transfer Learning. Water 10, 1485. doi:10.3390/w10101485. number: 10 Publisher: Multidisciplinary Digital Publishing Institute.

Johnson, J.M., Coll, J.M., Ruess, P.J., Hastings, J.T., 2018. Challenges and Opportunities for Creating Intelligent Hazard Alerts: The FloodHippo Prototype. Journal of the American Water Resources Association 54, 872–881. URL: https://onlinelibrary.wiley.com/doi/abs/10.1111/1752-1688.12645, doi:10.1111/1752-1688.12645.

Johnson, J.M., Munasinghe, D., Eyelade, D., Cohen, S., 2019. An integrated evaluation of the National Water Model (NWM)Height Above Nearest Drainage (HAND) flood mapping methodology. Natural Hazards and Earth System Sciences 19, 2405–2420. URL: https://nhess.copernicus.org/articles/19/2405/2019/, doi:10.5194/nhess-19-2405-2019.

Jongman, B., Ward, P.J., Aerts, J.C.J.H., 2012. Global exposure to river and coastal flooding: Long term trends and changes. Global Environmental Change 22, 823–835. doi:10.1016/j.gloenvcha.2012.07.004.

Jonkman, S.N., 2007. Loss of life estimation in flood risk assessment; theory and applications. Ph.D. thesis. TU Delft.

Jordahl, K., den Bossche, J.V., Fleischmann, M., Wasserman, J., McBride, J., Gerard, J., Tratner, J., Perry, M., Badaracco, A.G., Farmer, C., et al., 2020. geopandas/geopandas: v0.8.1. URL: `https://doi.org/10.5281/zenodo.3946761`, doi:`10.5281/zenodo.3946761`.

Kramer, M., Terheiden, K., Wieprecht, S., 2016. Safety criteria for the trafficability of inundated roads in urban floodings. International Journal of Disaster Risk Reduction 17, 77–84. URL: `https://linkinghub.elsevier.com/retrieve/pii/S2212420915301783`, doi:`10.1016/j.ijdrr.2016.04.003`.

Landuyt, L., Van Wesemael, A., Schumann, G.J.P., Hostache, R., Verhoest, N.E., Van Coillie, F.M., 2018. Flood mapping based on synthetic aperture radar: An assessment of established approaches. IEEE Transactions on Geoscience and Remote Sensing 57, 722–739.

Latto, A., Berg, R., 2020. Tropical Cyclone Report Tropical Storm Imelda (AL112019) 1719 September 2019. Technical Report. National Hurricane Center.

Leskovec, J., Sosič, R., 2016. SNAP: A general-purpose network analysis and graph-mining library. ACM Transactions on Intelligent Systems and Technology (TIST) 8, 1–20.

Levy, B.S., Patz, J.A., 2015. Climate Change, Human Rights, and Social

Justice. Annals of Global Health 81, 310. doi:10.1016/j.aogh.2015.08.008.

Lo, S.W., Wu, J.H., Lin, F.P., Hsu, C.H., 2015. Visual Sensing for Urban Flood Monitoring. Sensors 15, 20006–20029. doi:10.3390/s150820006. number: 8 Publisher: Multidisciplinary Digital Publishing Institute.

Maples, L.Z., Tiefenbacher, J.P., 2009. Landscape, development, technology and drivers: The geography of drownings associated with automobiles in Texas floods, 19502004. Applied Geography 29, 224–234. doi:10.1016/j.apgeog.2008.09.004.

Martnez-Gomariz, E., Gmez, M., Russo, B., Djordjevi, S., 2017. A new experiments-based methodology to define the stability threshold for any vehicle exposed to flooding. Urban Water Journal 14, 930–939. URL: https://www.tandfonline.com/doi/full/10.1080/1573062X.2017.1301501, doi:10.1080/1573062X.2017.1301501.

Martnez-Gomariz, E., Gmez, M., Russo, B., Djordjevi, S., 2018. Stability criteria for flooded vehicles: a state-of-the-art review: Stability criteria for flooded vehicles. Journal of Flood Risk Management 11, S817–S826. URL: https://onlinelibrary.wiley.com/doi/10.1111/jfr3.12262, doi:10.1111/jfr3.12262.

Ming, X., Liang, Q., Xia, X., Li, D., Fowler, H.J., 2020. Real-Time Flood Forecasting Based on a High-Performance 2-D Hydrodynamic Model and Numerical Weather Predictions. Water Resources

Research 56, e2019WR025583. doi:10.1029/2019WR025583. _eprint: https://onlinelibrary.wiley.com/doi/pdf/10.1029/2019WR025583.

Mioc, D., Nkhwanana, J., Moreiri, K., Nickerson, B., Santos, M., McGillivray, E., Morton, A., Anton, F., Ahmad, A., Mezouaghi, M., Mofford, L., Tang, P., 2015. Natural and man-made flood risk mapping and warning for socially vulnerable populations. International Journal of Safety and Security Engineering 5, 183–202. doi:10.2495/SAFE-V5-N3-183-202.

Morsy, M.M., Goodall, J.L., O'Neil, G.L., Sadler, J.M., Voce, D., Hassan, G., Huxley, C., 2018. A cloud-based flood warning system for forecasting impacts to transportation infrastructure systems. Environmental Modelling & Software 107, 231–244. doi:10.1016/j.envsoft.2018.05.007.

Mudashiru, R.B., Sabtu, N., Abustan, I., Balogun, W., 2021. Flood hazard mapping methods: A review. Journal of Hydrology 603, 126846. doi:10.1016/j.jhydrol.2021.126846.

Nash, J., Sutcliffe, J., 1970. River flow forecasting through conceptual models part I A discussion of principles. Journal of Hydrology 10, 282–290. doi:10.1016/0022-1694(70)90255-6.

National Oceanic and Atmospheric Administration, 2016. National water model: Improving noaas water prediction services. URL: https://water.noaa.gov/documents/wrn-national-water-model.pdf.

National Weather Service, 2022. National Weather Service Radar. URL: https://radar.weather.gov. (Last Accessed: 2021-06-16).

Natural Resources Conservation Service, 2023. Soil Survey Geographic Database (SSURGO). URL: https://websoilsurvey.nrcs.usda.gov/. (Last Accessed: 2023-04-27).

Naulin, J.P., Payrastre, O., Gaume, E., 2013. Spatially distributed flood forecasting in flash flood prone areas: Application to road network supervision in Southern France. Journal of Hydrology 486, 88–99. Publisher: Elsevier.

Nielsen, E.R., Schumacher, R.S., 2020. Dynamical Mechanisms Supporting Extreme Rainfall Accumulations in the Houston Tax Day 2016 Flood. Monthly Weather Review 148, 83–109. doi:10.1175/MWR-D-19-0206.1.

OpenStreetMap contributors, 2017. Planet dump retrieved from https://planet.osm.org . https://www.openstreetmap.org.

Panakkal, P., Juan, A., Garcia, M., Padgett, J.E., Bedient, P., 2019. Towards enhanced response: Integration of a flood alert system with road infrastructure performance models, in: Structures Congress 2019: Buildings and Natural Disasters, American Society of Civil Engineers Reston, VA. pp. 294–305.

Panakkal, P., Price, A., Padgett, J., Bedient, P., 2022. Opensafe mobility. https://github.com/Pranavesh-Panakkal/OpenSafe-Mobility. (Last Accessed: 2022-10-04).

Perica, S., Pavlovic, S., St. Laurent, M., Trypaluk, C., Unruh, D., Wilhite, O., 2018. Precipitation-Frequency Atlas of the United States. Volume 11, Version 2.0. Texas. doi:10.25923/1ceg-5094.

Perks, M.T., Russell, A.J., Large, A.R., 2016. Advances in flash flood monitoring using unmanned aerial vehicles (UAVs). Hydrology and Earth System Sciences 20, 4005–4015. Publisher: Copernicus GmbH.

Praharaj, S., Zahura, F.T., Chen, T.D., Shen, Y., Zeng, L., Goodall, J.L., 2021. Assessing Trustworthiness of Crowdsourced Flood Incident Reports Using Waze Data: A Norfolk, Virginia Case Study. Transportation Research Record 2675, 650–662. URL: https://doi.org/10.1177/03611981211031212, doi:10.1177/03611981211031212. publisher: SAGE Publications Inc.

Pregnolato, M., Ford, A., Glenis, V., Wilkinson, S., Dawson, R., et al., 2017. Impact of climate change on disruption to urban transport networks from pluvial flooding. Journal of Infrastructure Systems 23, 04017015.

Pyatkova, K., Chen, A.S., Butler, D., Vojinovi, Z., Djordjevi, S., 2019. Assessing the knock-on effects of flooding on road transportation. Journal of Environmental Management 244, 48–60. doi:10.1016/j.jenvman.2019.05.013.

Rapidlasso GmbH, 2012. LAStools. URL: https://rapidlasso.com/lastools/. (Last Accessed: 2022-03-27).

Ravuri, S., Lenc, K., Willson, M., Kangin, D., Lam, R., Mirowski, P., Fitzsimons, M., Athanassiadou, M., Kashem, S., Madge, S., et al., 2021. Skilful precipitation nowcasting using deep generative models of radar. Nature 597, 672–677.

Robinson, A.C., Chen, J., Lengerich, E.J., Meyer, H.G., MacEachren, A.M., 2005. Combining Usability Techniques to Design Geovisualization Tools for Epidemiology. Cartography and geographic information science 32, 243–255. URL: https://www.ncbi.nlm.nih.gov/pmc/articles/PMC2786201/, doi:10.1559/152304005775194700.

Sebastian, A., Lendering, K., Kothuis, B., Brand, A., Jonkman, S., Gelder, P., Kolen, B., Comes, T., Lhermitte, S., Meesters, K., Walle, B., Ebrahimi Fard, A., Cunningham, S., Khakzad, N., Nespeca, V., 2017. Hurricane Harvey Report: A fact-finding effort in the direct aftermath of Hurricane Harvey in the Greater Houston Region.

Shand, T., Cox, R., Blacka, M., Smith, G., 2011. Australian rainfall and runoff (ar&r). revision project 10: Appropriate safety criteria for vehicles; report number: P10/s2/020. Water Research Laboratory, The University of New South Wales: Manly Vale, Australia .

Stern, R.E., Song, J., Work, D.B., 2017. Accelerated Monte Carlo system reliability analysis through machine-learning-based surrogate models of network connectivity. Reliability Engineering & System Safety 164, 1–9. doi:10.1016/j.ress.2017.01.021.

Sumalee, A., Ho, H.W., 2018. Smarter and more connected: Future intelligent transportation system. IATSS Research 42, 67–71. doi:10.1016/j.iatssr.2018.05.005.

Texas Department of Transportation, 2022. Texas Department of Transportation - DriveTexas. URL: https://drivetexas.org. (Last Accessed: 2022-03-15).

TranStar, H., 2022. Houston TranStar - Traffic Map. URL: https://traffic.houstontranstar.org/layers/. (Last Accessed: 2022-03-27).

Twitter, Inc., 2022. Twitter. URL: https://twitter.com/home. (Last Accessed: 2022-03-26).

U.S. Census Bureau, 2022. 2022 tiger/line shapefiles: Census tracts. URL: https://www.census.gov/cgi-bin/geo/shapefiles/index.php. (Last Accessed: 2023-05-01).

U.S. Department of Homeland Security, 2022. Homeland Infrastructure Foundation-Level Data (HIFLD). URL: https://hifld-geoplatform.opendata.arcgis.com/. (Last Accessed: 2022-03-27).

U.S. Geological Survey, 2022a. Flood Event Viewer - Hurricane Harvey. URL: https://stn.wim.usgs.gov/fev/#HarveyAug2017. (Last Accessed: 2022-03-27).

U.S. Geological Survey, 2022b. USGS Water Data for the Nation. URL: https://waterdata.usgs.gov/nwis. (Last Accessed: 2022-03-27).

U.S. Geological Survey, 2023. The National Map. URL: https://apps.nationalmap.gov/downloader/#/. (Last Accessed: 2023-04-27).

Versini, P.A., Gaume, E., Andrieu, H., 2010. Application of a distributed hydrological model to the design of a road inundation warning system for flash flood prone areas. Natural Hazards and Earth System Sciences 10, 805–817. doi:10.5194/nhess-10-805-2010. publisher: Copernicus GmbH.

Vieux & Associates, Inc., 2022. About Gauge Adjusted Radar Rainfall (GARR). URL: https://www.vieuxinc.com/gauge-adjusted-radar-rainfall-garr/. (Last Accessed: 2021-10-20).

Viikari, V.V., Varpula, T., Kantanen, M., 2009. Road-Condition Recognition Using 24-GHz Automotive Radar. IEEE Transactions on Intelligent Transportation Systems 10, 639–648. doi:10.1109/TITS.2009.2026307.

Wickham, J., Stehman, S.V., Sorenson, D.G., Gass, L., Dewitz, J.A., 2021. Thematic accuracy assessment of the NLCD 2016 land cover for the conterminous United States. Remote Sensing of Environment 257, 112357. doi:10.1016/j.rse.2021.112357.

Winsemius, H.C., Aerts, J.C.J.H., van Beek, L.P.H., Bierkens, M.F.P., Bouwman, A., Jongman, B., Kwadijk, J.C.J., Ligtvoet, W., Lucas, P.L., van Vuuren, D.P., Ward, P.J., 2016. Global drivers of future river flood risk. Nature Climate Change 6, 381–385. doi:10.1038/nclimate2893. number: 4 Publisher: Nature Publishing Group.

Yin, J., Yu, D., Lin, N., Wilby, R.L., 2017. Evaluating the cascading impacts of sea level rise and coastal flooding on emergency response spatial accessibility in Lower Manhattan, New York City. Journal of Hydrology 555, 648–658. URL: https://www.sciencedirect.com/science/article/pii/S0022169417307321, doi:10.1016/j.jhydrol.2017.10.067.

Zhang, W., Villarini, G., Vecchi, G.A., Smith, J.A., 2018. Urbanization exacerbated the rainfall and flooding caused by hurricane Harvey in Houston. Nature 563, 384–388. doi:10.1038/s41586-018-0676-z. number: 7731 Publisher: Nature Publishing Group.

Zhu, L., Yu, F.R., Wang, Y., Ning, B., Tang, T., 2019. Big Data Analytics in Intelligent Transportation Systems: A Survey. IEEE Transactions on Intelligent Transportation Systems 20, 383–398. doi:10.1109/TITS.2018.2815678.